AGU PUBLICATIONS

Tectonics

RESEARCH ARTICLE
10.1002/2015TC003926

Key Points:
- The SSA was a passive margin on the north side of the Neotethys Ocean in the Permian and Triassic
- Subduction and arc magmatism began in latest Triassic/Early Jurassic time, culminating at ~170 Ma
- Ophiolites on either side of the zone are of different origins

Correspondence to:
J. Hassanzadeh,
jamshid@caltech.edu

Citation:
Hassanzadeh, J., and B. P. Wernicke (2016), The Neotethyan Sanandaj-Sirjan zone of Iran as an archetype for passive margin-arc transitions, *Tectonics*, *35*, 586–621, doi:10.1002/2015TC003926.

Received 15 MAY 2015
Accepted 2 FEB 2016
Accepted article online 6 FEB 2016
Published online 11 MAR 2016

The Neotethyan Sanandaj-Sirjan zone of Iran as an archetype for passive margin-arc transitions

Jamshid Hassanzadeh[1] and Brian P. Wernicke[1]

[1]Division of Geological and Planetary Sciences, California Institute of Technology, Pasadena, California, USA

Abstract The Sanandaj-Sirjan zone of Iran is a northwest trending orogenic belt immediately north of the Zagros suture, which represents the former position of the Neotethys Ocean. The zone contains the most extensive, best preserved record of key events in the formation and evolution of the Neotethys, from its birth in Late Paleozoic time through its demise during the mid-Tertiary collision of Arabia with Eurasia. The record includes rifting of continental fragments off of the northern margin of Gondwanaland, formation of facing passive continental margins, initiation of subduction along the northern margin, and progressive development of a continental magmatic arc. The latter two of these events are critical phases of the Wilson Cycle that, elsewhere in the world, are poorly preserved in the geologic record because of superimposed events. Our new synthesis reaffirms the similarity between this zone and various terranes to the north in Central Iran. Late Paleozoic rifting, preserved as A-type granites and accelerated subsidence, was followed by a phase of pronounced subsidence and shallow marine sedimentation in Permian through Triassic time, marking the formation and evolution of passive margins on both sides of the suture. Subduction and arc magmatism began in latest Triassic/Early Jurassic time, culminating at ~170 Ma. The extinction of arc magmatism in this zone, and its shift northeastward to form the subparallel Urumieh-Dokhtar arc, occurred diachronously along strike, in Late Cretaceous or Paleogene time. Post-Cretaceous uplift transformed the zone from a primarily marine borderland into a marine archipelago that persisted until mid-Tertiary time.

1. Introduction

The Sanandaj-Sirjan zone is a region of polyphase deformation on the southwestern margin of Eurasia. It fringes Central Iran and is juxtaposed against the Arabian subcontinent (Zagros Mountains) along the Main Zagros thrust, hereafter "MZT" (Figure 1) [*Stöcklin*, 1968; *Takin*, 1972]. Its boundaries on either side are marked with discontinuously preserved ophiolites including the following: (1) the Neyriz-Kermanshah ophiolite (also known as the "outer belt") situated on the northern edge of the Zagros Mountains and (2) the Khoy and Nain-Baft ophiolite complexes to the northeast (part of the "inner belt" ophiolites) [*Stöcklin*, 1981] (Figure 1). The ophiolites are interposed with various tectonic elements of continental affinity within the broader Arabian-Eurasian collision zone, including the Alborz Mountains, Central Iran, central-east Iranian microplate (CEIM), and the Sanandaj-Sirjan zone to the north of the MZT, and the Zagros fold-thrust belt south of it (Figure 1). The ophiolites are generally regarded as preserving a record of an ocean basin or basins that lay between these elements in Mesozoic through mid-Cenozoic time, as a whole referred to as the Neotethys Ocean, with the Eurasian continent to the north, and Gondwanaland to the south [e.g., *Stöcklin*, 1974; *Sengör*, 1979; *Berberian and King*, 1981; *Stampfli and Borel*, 2002; *Agard et al*., 2011].

The general history of Eurasia and Gondwanaland from Permian to Recent times is defined by the rifting of continental fragments from the northern margin of Gondwanaland, and the accretion to the southern margin of Eurasia, the most salient example being the Indian subcontinent. A more subtle, early example to the west is the Cimmerian "continental ribbon," now represented by the various continental blocks in Iran north of the MZT. Cimmeria is generally thought to have separated from Gondwanaland in the Permian, forming the Neotethys Ocean [*Sengör*, 1979]. Most of the debate about the formation, evolution, and ultimate closure of the Neotethys Ocean therefore focuses on the geological details of both the ophiolites and the intervening continental elements in Iran.

In this paper, we focus on the general history of the Sanandaj-Sirjan zone, because in contrast to the Alborz, Central Iran, CEIM, and Zagros fold belt, it contains an extensive Mesozoic record of magmatism and metamorphism and is localized along the MZT, which is traditionally regarded as the main suture zone representing the Neotethys Ocean. The abbreviation "SSZ" is commonly used in the literature to denote this

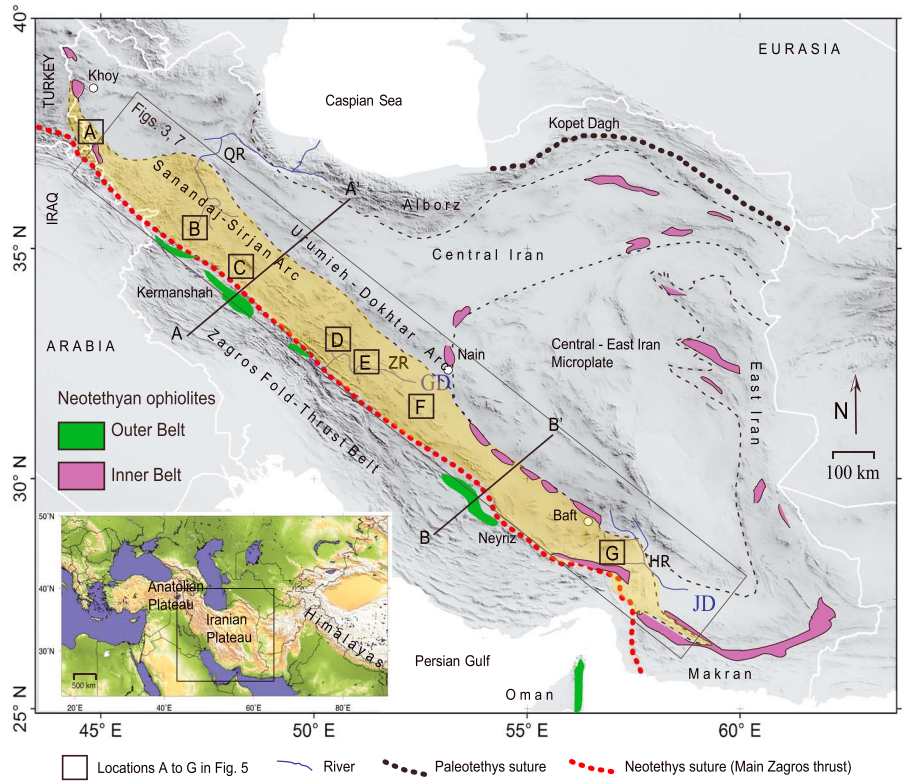

Figure 1. Map showing context of Sanandaj-Sirjan arc (yellow shading) within the broader Alpine-Himalayan collision zone (inset) and first-order tectonic elements of the Iranian Plateau, showing lines of sections A-A′ and B-B′ for Figure 10c, the locations of maps in Figures 3 and 7 (black box), stratigraphic columns in Figure 5 (squares labeled A to G), location of Paleotethyan and Neotethyan sutures (thick dashed lines), major boundaries of continental fragments (thin dashed lines), and ophiolite bodies (colored areas). Abbreviations: QR, Qezel Ozan-Sefidrud River; ZR, Zayandehrud River; HR, Halilrud River; GD, Gavkhooni depression; and JD, Jazmurian depression.

zone, but the same abbreviation is widely used in the geodynamics literature for "Supra Subduction Zone." To avoid confusion, we instead use either the acronym "SSA," after the Mesozoic Sanandaj-Sirjan arc, or simply "the zone."

The SSA represents the "core zone" or "metamorphic core" of the Arabia-Eurasia collision zone, but the general lack of isotopic dating has been a significant impediment to understanding the evolution of the collision zone in general. In particular, the issue of whether any of the magmatism or metamorphism present in the zone is related to the collision process, as in the western Alps or Himalayas, has remained unresolved, leading some authors to speculate that the SSA originally lay to the south of, rather than north of, the main Neotethys Ocean prior to collision, representing the partially subducted leading edge of the Arabian plate, structurally beneath the inner and outer ophiolite belts [e.g., *Alavi*, 1994; *Shafaii Moghadam and Stern*, 2011]. Arc magmatism is the most distinctive component of the SSA, which includes voluminous calc-alkaline plutons and volcanic rocks, mainly of Jurassic age, which as demonstrated below culminated around 170 Ma. The Jurassic magmatism differentiates the SSA from the Zagros fold and thrust belt to the southwest, which was amagmatic during the Jurassic. It also differentiates it from various elements in Central Iran to the northeast (exclusive of the central-east Iran microplate, Figure 1), which contain only sparse igneous rocks of Jurassic age.

Here, we synthesize (1) extensive geological mapping of the zone, published from the early 1960s up to the present day; (2) stratigraphic data, particularly in Permain through Jurassic strata in the region; and (3) key aspects of the recent growing geochemical and geochronological database (e.g., >1100 individual zircon age determinations in igneous rocks of the SSA completed over the last decade), to systematically address a number of important questions as regards the tectonic setting of the SSA in the Neotethyan realm. We identify seven specific questions, around which current debate on the role of the SSA within the

Neotethyan paleogeographic realm is centered, and address each of them in the last section of the paper on the basis of our synthesis. These questions include the following: (1) What are its similarities and differences in the evolution of the SSA and various domains to the north? (2) Did the inner and outer belt ophiolites form in the same oceanic domain (relative to the SSA) or in separate domains on either side of the SSA? (3) The position of the arc—Did the SSA lie on the southern margin of the Neotethyan Ocean, or was it part of the Cimmerian continental ribbon on the northern side of the Neotethys Ocean? (4) What was the polarity of Neotethyan subduction? (5) Is there compelling evidence for rifting and the formation of a passive margin in Permian time? (6) What is the evidence for, and extent of, the development of a calc-alkaline magmatic arc subsequent to passive margin development? And (7) is metamorphism in the zone primarily the result of high heat flux during arc magmatism, or some other process? Resolution of these issues will bear on what we regard as the most fundamental question raised by the SSA: Is it among the best (if not the best) records of a transition from a passive continental margin to a continental arc?

2. Tectonic Setting

The SSA is the southernmost tectonostratigraphic element or terrane north of the MZT (Figure 1). In geographic terms, it is included in the Zagros Mountains because of similar elevations and the parallelism in the structural grain of the two belts. However, its post-Triassic geology markedly differs from the Zagros fold and thrust (ZFT) belt, as we elaborate below. The belt is about 100–150 km wide and runs parallel to the ZFT for ~1500 km. Most maps delimit the SSA on the northwest in the Iran-Iraq-Turkey border region (Turkish-Iranian Plateau) and on the southeast by the east Zagros syntaxis at the Strait of Hormuz. This relatively narrow definition overlooks one of the most significant discoveries of the East Iran Project in the 1970s, which is the continuation of the SSA as an east tapering wedge or "tail" in the accretionary prism of the Makran belt, well to the east of the syntaxis [*McCall and Kidd*, 1982; *McCall*, 1985, 2002]. The continuation of the Jurassic SSA southeast of the Strait of Hormuz into the Makran belt has more recently been confirmed with detailed field work and U/Pb geochronology on granitic and trondjemitic plutonic rocks from the Dur Kan complex, which yield ages of 175–163 Ma, with variable amounts of continental influence in the magmatic source regions [*Hunziker et al.*, 2015]. Including the tail, the zone is more than 2000 km long (Figure 1), longer in dimensions than the Late Cretaceous arc in the U.S. Cordillera between southern California and the Canadian border.

Within the arc, postmagmatic episodes of both contractile and extensional tectonics are documented, and therefore, the width of the arc may have been significantly modified by these events. However, there is as yet no evidence of major (San Andreas type) strike-slip faulting or orogen-parallel strain events that would have modified its dimensions so as to omit or duplicate large (>100 km) segments of the original arc [*Stöcklin and Nabavi*, 1973; *Berberian and King*, 1981]. Significant postarc tectonic events clearly affected the northern margin of the Neotethys Ocean [*Agard et al.*, 2011; *Mohajjel and Fergusson*, 2014]. For example, the possibility exists that much of the Central Iran domain (NW Iran and the central-east Iran microplate), now to its NE, was transported via large-scale left-lateral strike-slip faulting in the Cretaceous, from a position originally along orogenic strike to the SE to its current position, effectively "doubling up" the width of the arc [e.g., *Sengör*, 1990, Figure 6]. However, even in the context of this mobilistic synthesis, the SSA as presently defined in Iran is regarded as a single paleogeographic entity within the Neotethyan realm, with the approximate continuity and width of a typical modern arc [*Berberian and Berberian*, 1981; *Kazmin et al.*, 1986; *Agard et al.*, 2006; *Chiu et al.*, 2013].

From latest Cretaceous time until the mid-Tertiary collision of the Arabian and Eurasian continents (circa 30–20 Ma) [*McQuarrie et al.*, 2003], a major flare-up of arc magmatism affected large parts of Iran NW of the SSA, forming the Urumieh-Dokhtor arc (Figure 1). Peak magmatism in the arc occurred between 55 and 35 Ma and was relatively minor thereafter [*Verdel et al.*, 2011]. The SSA lay in the fore-arc region during this time and, largely avoided magmatic or metamorphic overprint that might otherwise have occurred, had the two arcs formed in the same place.

Early estimates of crustal thickness of the Iranian Plateau beneath the SSA of up to 64 km have been interpreted to indicate a doubling of the crustal thickness from south to north across the Zagros suture [e.g., *Dehghani and Makris*, 1984; *Giese et al.*, 1984, Figure 7]. More recently, several seismic imaging projects across the Zagros orogen were attempted to test the hypothesis of a thick crustal root beneath the SSA. *Paul et al.* [2010] and *Hatzfeld and Molnar* [2010] concluded that there was not more than 10 km of

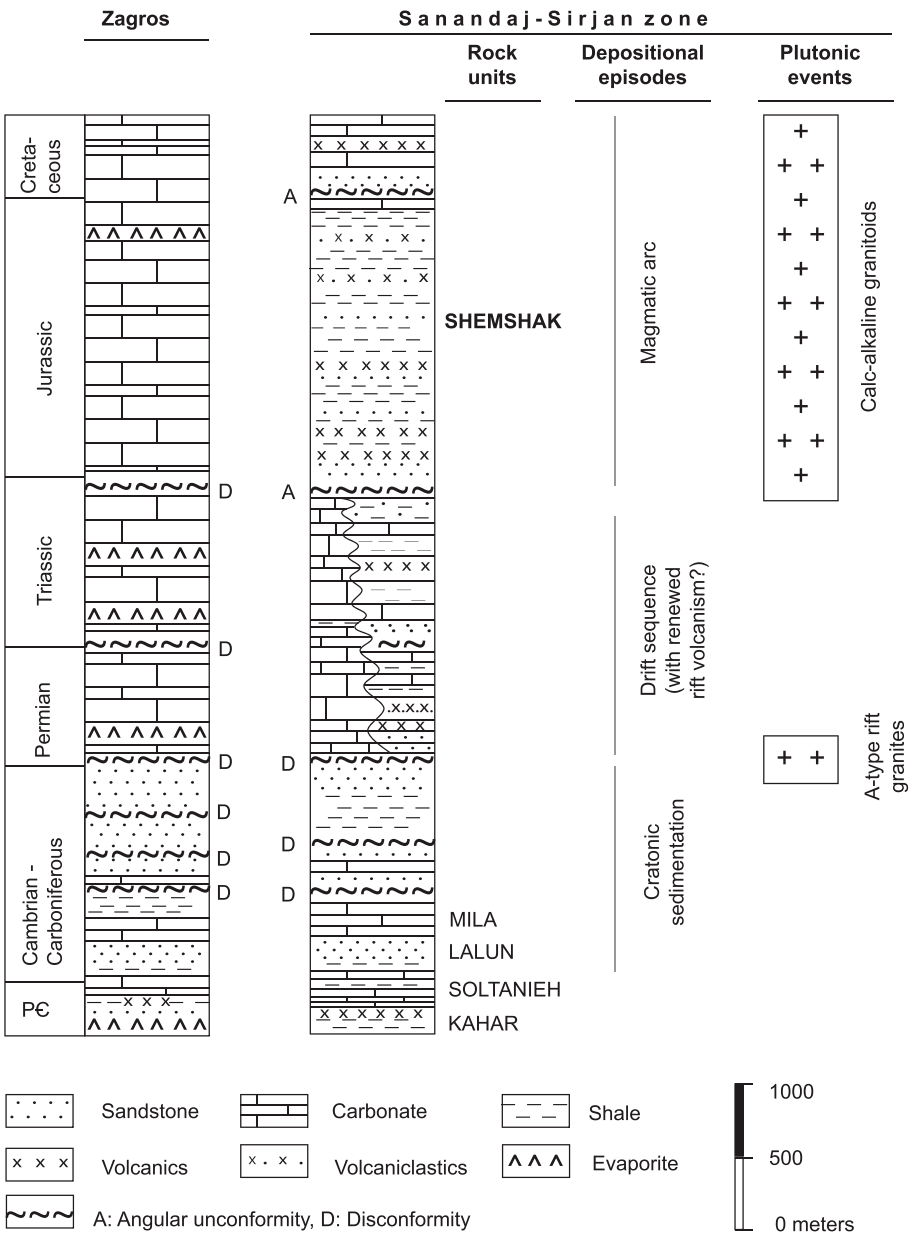

Figure 2. Comparison of generalized stratigraphic sections and tectonomagmatic events for late Neoproterozoic through Early Cretaceous time for the Sanandaj-Sirjan zone and the Zagros fold-thrust belt. Thicknesses of some units, especially those of Precambrian and Paleozoic age, are locally much greater than shown.

northward thickening (maximum thickness approximately 40–50 km) under the SSA relative to the surrounding lowlands but did not rule out the possibility of localized belts with deeper roots. On the other hand, *Tatar and Nasrabadi* [2013] verified a Moho depth of ~58 km below the NW part of the SSA. The GPS-derived velocity field suggests that at present, the SSA is moving as an internally rigid block 14 to 16 mm/yr northward relative to the Asian interior, with a modest component of counterclockwise rotation [e.g., *Vernant et al.*, 2004; *Reilinger and McClusky*, 2011].

3. Stratigraphic Record

Stratigraphy is the primary discriminant between the tectonic context of various crustal blocks within the Neothyan Ocean and the primary factor in the practical question of the internal coherence of any given

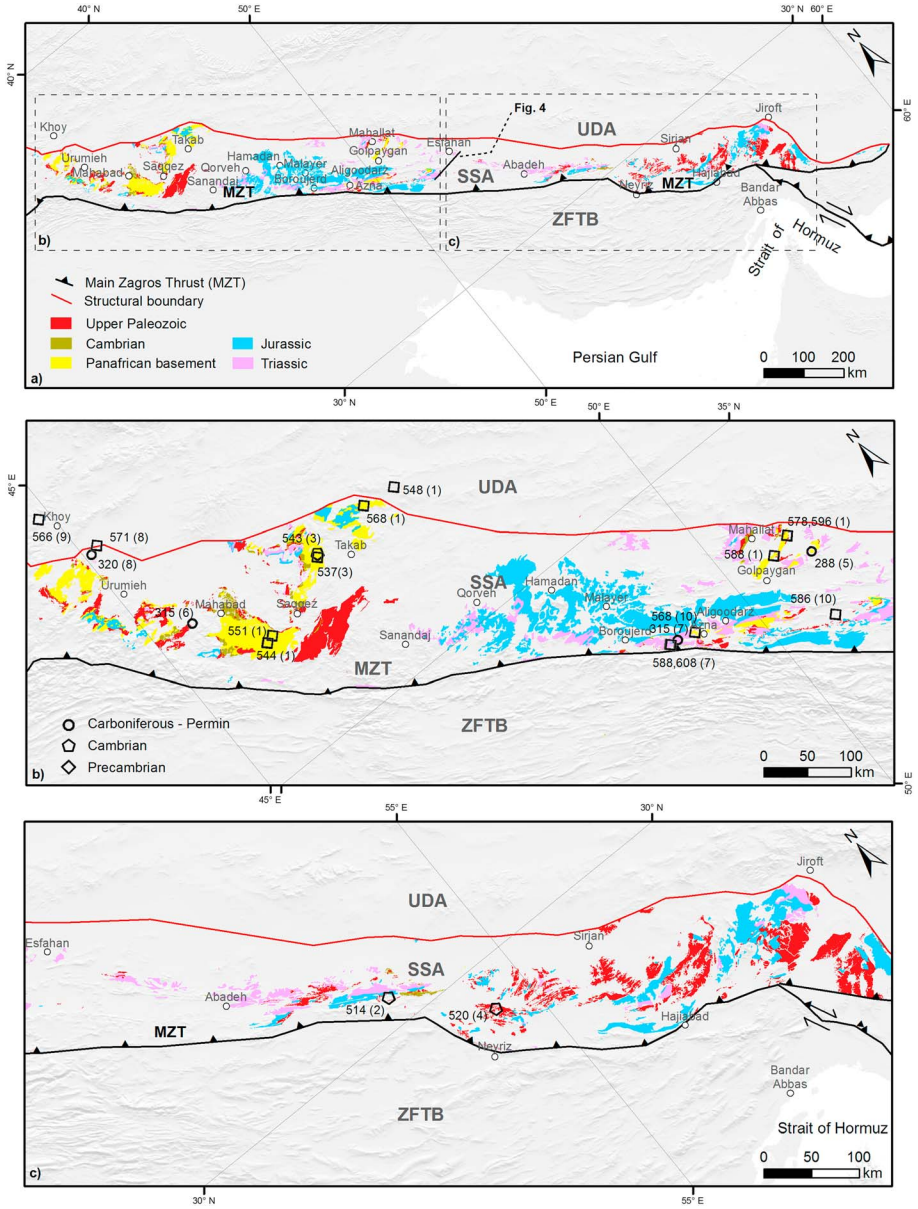

Figure 3. Geographic distribution of Precambrian-Cambrian cratonic basement, younger Paleozoic platform cover, passive margin deposits of Permian and Triassic age, and arc sequences of Jurassic age. Black symbols show radiometric ages of Precambrian and Paleozoic igneous rocks; sources of data: (1) *Hassanzadeh et al*. [2008], (2) *Hosseini et al*. [2012], (3) *Jamshidi Badr et al*. [2010], (4) *Sheikholeslami et al*. [2008], (5) *Alirezaei and Hassanzadeh* [2012], (6) *Bea et al*. [2011], (7) *Shakerardakani et al*. [2015], (8) *Shafaii Moghadam et al*. [2015], (9) *Azizi et al*. [2011c], and (10) *Nutman et al*. [2014].

block. We therefore briefly review the major pre-Cenozoic sequences in order to shed light on the existing controversies surrounding the tectonic setting of the zone within and along the margins of the Neotethys Ocean (Figure 2). We also present a new, large-scale geologic map of the SSA (Figures 3 and 7), showing the distribution of major pre-Cretacous rock units, based on a compilation of geologic mapping in the SSA. Sources for the new map include (1) 1:250,000-scale maps largely published in the mid-1980s or earlier, (2) a significant number of 1:100,000-scale maps currently being produced by the Geological Survey of Iran, supplemented by (3) more detailed studies published in journal articles and (4) by our own field observations. These maps represent the first major revision of the large-scale distribution of major pre-Cretaceous rock units in the SSA since the compilation of *Haghipour and Aghanabati* [1989].

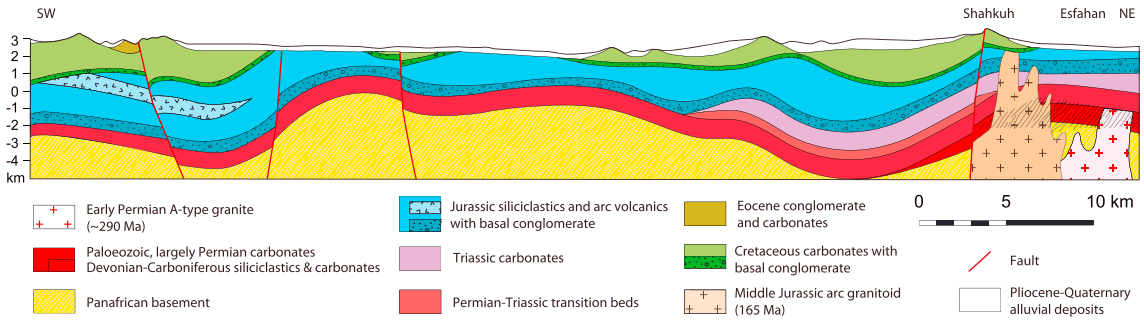

Figure 4. Typical cross section of the Sanandaj-Sirjan zone near Esfahan, with pre-Cretaceous units color coded to the geologic maps (Figures 3 and 7). Pre-Jurassic structural and stratigraphic relationships are based on down-plunge projections from nearby surface exposures. Among the sedimentary rock units the basal conglomerates of Jurassic and Cretaceous sequences are highlighted because they represent important orogenic events in the evolution of the continental arc along the northern margin of the Neotethys Ocean. Section modified from *Zahedi* [1976].

3.1. Pre-Jurassic Strata

Pre-Mesozoic rocks, both stratified and crystalline, are relatively sparsely exposed compared with younger formations (Figure 3). They are typical of other units in the north-central portion of Gondwanaland, especially pre-Permian rocks. It forms a substrate of cratonic basement upon which later passive margin and arc components of the collision zone were able to develop. It includes (1) a latest Proterozoic-Cambrian continental basement assemblage of coalesced magmatic arcs, overlain by (2) thin, concordant, disconformity-bound platform cover sequences of Paleozoic age (Figure 2) [*Thiele et al*., 1968; *Stöcklin*, 1968, 1974; *Berberian and King*, 1981; *Eftekharnezhad*, 2004; *Hassanzadeh et al*., 2008]. The largest exposures of these rocks lie near the Mahabad-Takab and Golpaygan-Mahallat regions (Figure 3), previously described by *Eftekharnezhad* [2004] and *Thiele et al*. [1968]. They exhibit close stratigraphic similarities, at formation scale and below, to sections located northeast of the SSA, including in the Soltanieh Mountains (NW part of the Urumieh-Dokhtar arc), the Alborz Mountains, and central-east Iran microplate (Figure 1) [*Stöcklin*, 1968].

The section near Mahabad is typical (Figure 3): The Kahar Formation is the oldest of the unmetamorphosed rock units and consists of up to 1200 m of micaceous shales and siliceous tuffs of uncertain stratigraphic relationship with adjacent crystalline complexes, which exhibit a structural thickness of ~3000 m in the Takab region [*Alavi Naini et al*., 1982]. These are succeeded by as much as 2200 m of a relatively undisturbed sequence consisting of shales, felsic volcanics, dolostones, cherts, and sandstones representing the rock formations from the top of the Kahar Formation through the Cambrian Lalun Formation (Figures 3 and 4) [*Eftekharnezhad*, 2004]. Equivalent strata in the Alborz Mountains [*Horton et al*., 2008; *Etemad-Saeed et al*., 2015] have yielded detrital zircon ages from latest Neoproterozoic to Early Cambrian. The Lalun Formation is succeeded upsection by approximately 200 m of trilobite-bearing Mila Formation carbonates, shales, and sandstones. Permian marine strata unconformably overlie the Mila Formation, with a well-defined depositional contact. A similar Proterozoic-Paleozoic sequence occurs in the Golpaygan-Mahallat area, which in addition includes minor thicknesses of Carboniferous deposits (Figure 2) [*Thiele et al*., 1968].

The most complete, unmetamorphosed Permian-Triassic sections are exposed farther SE near Shahreza (south of Esfahan) and Abadeh (Figures 2, 5e, and 5f, respectively) [e.g., *Taraz*, 1974; *Heydari et al*., 2003]. Near Abadeh, Permian strata are underlain by ~400 m of Lower Carboniferous limestones and sandstones and ~1300 m of Upper Carboniferous (?) sandstones, limestones, dolostones, and shales. Concordantly overlying these strata are about 1200 m of Permian reefal and biomicritic strata [*Taraz*, 1974]. A transgressive basal Permian limestone contains an Artinskian faunal assemblage (~276 Ma). The Permian sequence is conformably overlain by ~2300 m of the Triassic limestones and dolostones [*Taraz*, 1974] and thus contains a valuable reference section for the Paleozoic-Mesozoic boundary [*Heydari et al*., 2003].

The Permian and Triassic sequence in the SSA is largely amagmatic. However, it locally contains significant volumes of mafic to bimodal volcanics of indeterminate age, due to alteration and metamorphism of potentially dateable material. The volcanic components include, from northwest to southeast (Figures 3 and 5), (1) bimodal metavolcanics underlying the Hamadan phyllites to the south and west of Hamadan (Figure 5c) [*Braud*, 1990; *Eshraghi*, 1996; *Jafarian and Zamani Pedram*, 1999]; (2) intermediate to mafic volcanics within pre-

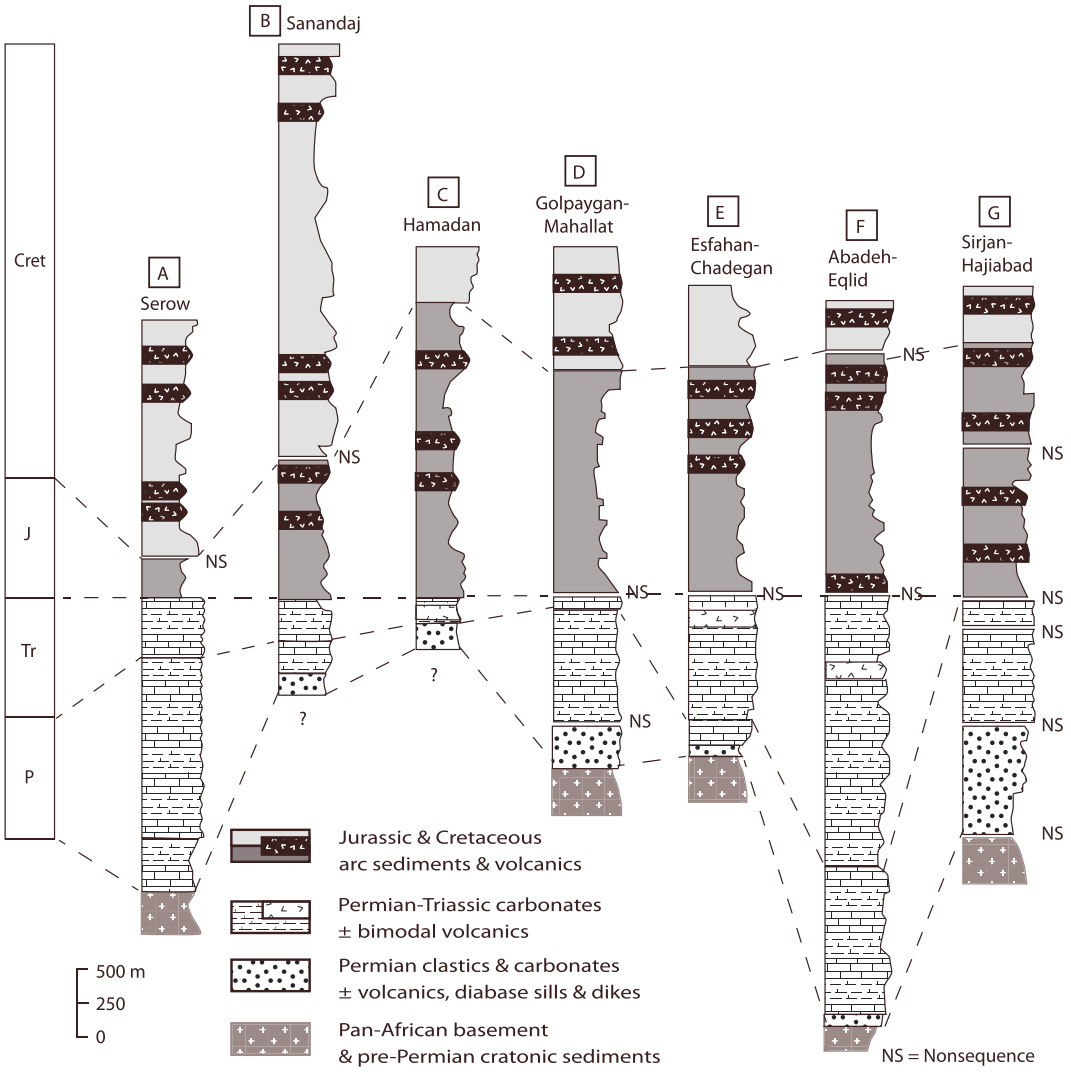

Figure 5. Representative stratigraphic columns showing Permian through Early Cretaceous strata. Locations are shown in Figure 1. Data are from published maps and reports of the Geological Survey of Iran referred to in text. NS (nonsequence) indicates that stratigraphic continuity is broken due to exposure.

Jurassic marbles between Golpaygan and the MZT, which have conflicting age attributions of either Permian (Figures 5d and 5e) [e.g., *Thiele et al*., 1968] or Triassic [*Mohajjel*, 1992; *Soheili et al*., 1992]; (3) submarine, bimodal lavas, and tuffs reported from the Abadeh area (Figure 5f) [*Taraz*, 1974; *Alric and Virlogeux*, 1977]; and (4) similar rocks of both Permian and Triassic age in the Sirjan area (Figure 5g) [*Dimitrijevic*, 1973; *Soffel et al*., 1996].

A salient aspect of the Permian-Triassic depositional system is that isopach maps of strata of this age define a "trough" centered on the MZT zone (Figure 6a) [e.g., *Edgell*, 1977]. A stratigraphic cross section shows the general southwestward thickening of Permian and Triassic strata from the Alborz to the Zagros suture (Figure 6b). These strata, deposited from Artinskian to Rhaetian time, are generally conformable, shallow marine carbonates and siliciclastics [e.g., *Taraz*, 1974] as much as 3500 m thick. Isopachs of Permian strata show that sequences on both the Arabian platform and across the Central Iran domain show the sections thickening by nearly a factor of 3 toward the suture, from a few hundred meters thick on the north and south extremes away from the suture, to more than a kilometer in sections within 200 km of the suture (Figure 6). Subsidence profiles of a representative section from the Abadeh region constructed by *Saidi et al*. [1997] captures modest subsidence during early Permian rifting and A-type granitic magmatism, followed by stronger subsidence from mid-Permian through Triassic time, with a convex-up tectonic subsidence profile suggestive of thermal subsidence (Figure 6c). More cratonic subsidence profiles also suggest a pulse of

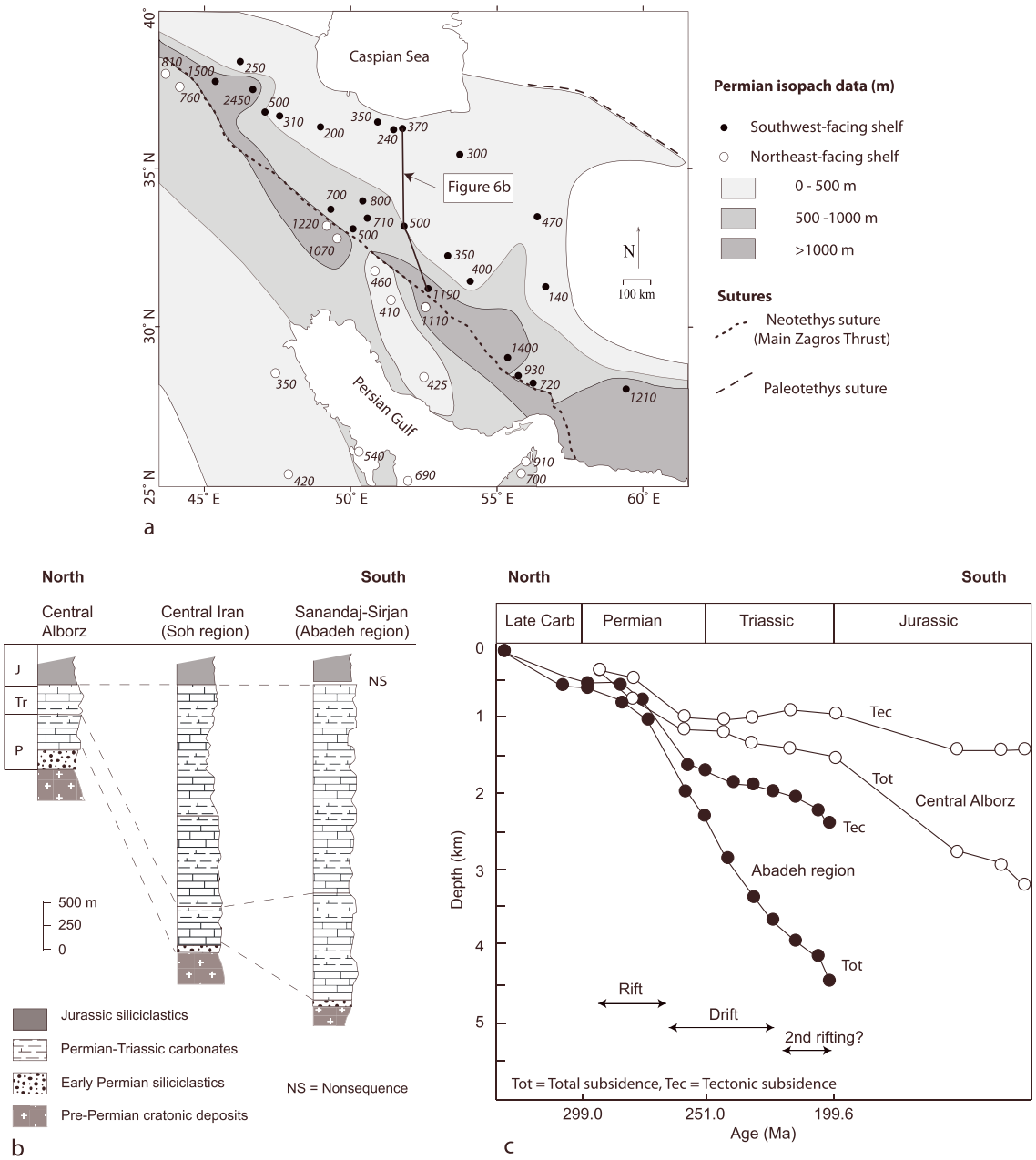

Figure 6. Permian-Triassic shelf carbonate sequences. (a) Isopach map of Permian carbonates across the Zagros suture from the Iranian plateau to the Arabian platform. (b) Stratigraphic diagram showing southward thickening of the Permian-Triassic shelf carbonates along a 600 km long north-south cross-section from the Alborz Mountains to the Sanandaj-Sirjan zone. Data are from *Stöcklin* [1972], *Taraz* [1974], *Edgell* [1977], *Zahedi* [1991], and published maps and reports of the Geological Survey of Iran referred to in text. (c) Total and tectonic subsidence curves for the Central Alborz and Abadeh region, marking an Early Permian rift event followed by a drifting event in the Late Permian through Triassic time (adopted from *Saidi et al.* [1997]).

tectonic subsidence beginning in mid-Permian time, followed by very gentle tectonic subsidence in the Triassic. The profiles suggest that renewed rifting and subsidence may have affected the northern margin of the Neotethys Ocean in Late Triassic and Jurassic time, perhaps due to renewed rifting just prior to the onset of Jurassic magmatism (Figure 6c).

3.2. Jurassic Strata

Jurassic strata occupy the largest surface area of bedrock outcrops in the SSA relative to those any other geologic period (Figure 7). The mostly Lower Jurassic (Liassic) Shemshak Formation rests above a regional

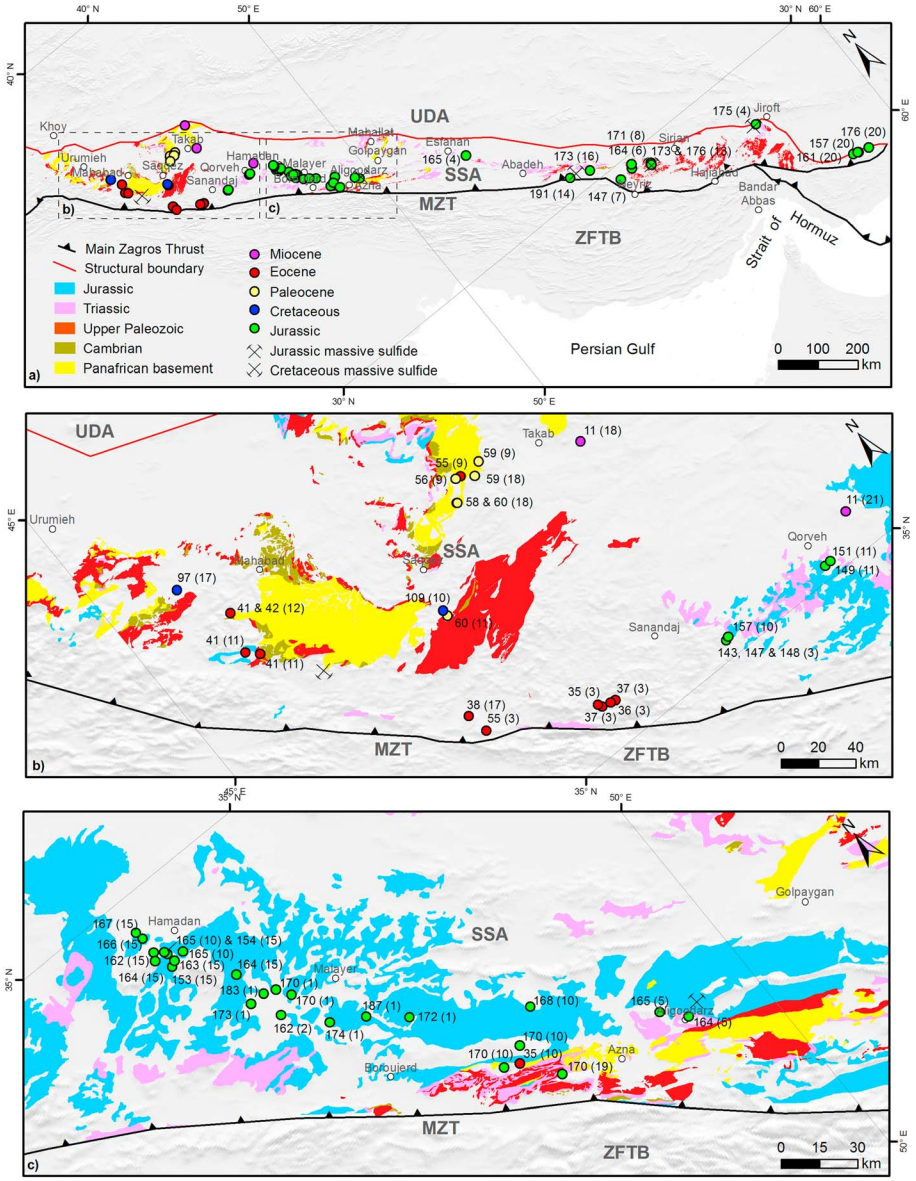

Figure 7. Geographic distribution of the Jurassic volcanosedimentry rock outcrops, Mesozoic and Tertiary plutons with U-Pb zircon ages, and Jurassic and Cretaceous massive sulfide deposits. Ages given in Ma, sources of data in parentheses, including the following: (1) *Ahadnejad et al.* [2011], (2) *Azizi et al.* [2011a], (3) *Azizi et al.* [2011b], (4) *Chiu et al.* [2013], (5) *Esna-Ashari et al.* [2012], (6) *Fazlnia et al.* [2007], (7) *Fazlnia et al.* [2009], (8) *Fazlnia et al.* [2013], (9) *Jamshidi Badr et al.* [2012], (10) *Mahmoudi et al.* [2011], (11) *Mazhari et al.* [2009], (12) *Mazhari et al.* [2011a], (13) *Mousivand et al.* [2011], (14) *Mousivand et al.* [2012], (15) *Shahbazi et al.* [2010], (16) *Hosseini et al.* [2012], (17) *Mazhari et al.* [2011b], (18) *Heidari* [2014], (19) *Shakerardakani et al.* [2015], (20) *Hunziker et al.* [2015], and (21) *Richards et al.* [2006].

post-Triassic unconformity and consists mainly of dark-hued, organic-rich, immature sandstones and shales, which are locally coal-bearing [*Aghanabati*, 2014] (Figures 3 and 5). A few intercalations of shallow marine strata occur in an otherwise continental (fluvial-deltaic) sequence. The Hamadan phyllites, with structural thicknesses of over 2000 m, are low greenschist facies equivalents of the Shemshak Formation (Figure 5c) [e.g., *Braud*, 1978; *Agard et al.*, 2005]. Throughout Iran, the Shemshak Formation contains volcaniclastic intercalations, and its sandstones tend to be rich in volcanic clasts. Two major distinctions exist between the SSA and the Arabian Zagros fold and thrust belt south of the MZT. The first is that south of the thrust, the Jurassic does not contain volcanic or volcaniclastic strata characteristic of the SSA (Figure 2). The second, described in more detail below, is that the Jurassic of the SSA was deformed and locally metamorphosed

prior to deposition of overlying Cretaceous strata, while no such Jura-Cretaceous events took place south of the thrust. The abundance of volcanics in the SSA (Figures 2 and 5) also contrasts with sections in the Alborz Mountains and Central Iran.

The Shemshak Formation and equivalents are in some areas succeeded by Middle to Late Jurassic siliciclastic and carbonate strata, which are most abundant to the south and the southeast of Sirjan where pelagic *Calpionella*-bearing limestones are also present near the top of the sequence [*Dimitrijevic*, 1973]. *Kazmin et al*. [1986] presented the first comprehensive compilation of the distribution of Jurassic calc-alkaline volcanic rocks along the SSA, with ages constrained mainly by intercalated fossil-bearing sediments. They were among the first to suggest a Japan-type island arc setting for the volcanism. Since then, radiometric dating has tended to underscore the importance of the arc, demonstrating that a number of volcano-sedimentary sequences of previously unknown affinity belong to the Jurassic arc assemblage.

In detail, the volcanic intercalations in the Shemshak Formation are complex and do not simply correlate from region to region. Occurrences of Jurassic volcanics are widespread and, from northwest to southeast, have been documented in the Sanandaj, Hamadan, Esfahan, Abadeh, and Sirjan areas (Figures 3–5). West of Hamadan, thick sequences of alternating volcanics, shales, and limestones, apparently interfingering with the Hamadan phyllites, have been mapped (Figure 5c) [*Braud*, 1990]. Southwest of Esfahan, occurrences of intermediate and felsic calc-alkaline volcanics within the Jurassic sequence have been described from along the Zayandehrud River (Figure 5e) [*Zahedi*, 1976, 1993]. Southeast of Abadeh, Lower Jurassic clastic sediments (Figures 5f and 7) are associated with a large area of greenschist facies metavolcanic and metasedimentary strata (Surian metamorphic complex, Table 1) previously believed to be Permo-Triassic or older [*Taraz*, 1974; *Houshmandzadeh and Soheili*, 1990]. However, metasandstones from this complex recently yielded U-Pb ages of 191 ± 12 Ma on detrital zircon. These data suggest an Early Jurassic or later depositional age for the sampled horizon [*Mousivand et al*., 2012] and increase the inventory of documented sections assigned to the Lower Jurassic arc. These authors have also suggested that the basaltic andesites have boninitic affinity. Similar to the case near Abadeh, greenschist facies rhyodacites and volcaniclastics northwest of Sirjan (Figures 5g and 7) [*Sabzehei et al*., 1993] have yielded Middle Jurassic U-Pb zircon ages [*Mousivand et al*., 2011]. Northeast of Neyriz, submarine basaltic lavas occur interlayered in Jurassic flysch [*Watters et al*., 1970]. Southeast of Sirjan and west of Jiroft, extensive mafic lavas of submarine origin associated with sandstones and tuffs reaching thicknesses of up to 2000 m have been identified nonconformably overlying metamorphic rocks of unknown age [*Grabeljsek et al*., 1972; *Timotijevic et al*., 1972; *Ghasemi et al*., 2002]. In the latter region basalts and andesites are abundant, and MORB-like and island arc tholeiitic signatures have been documented [*Monsef et al*., 2011]. These authors have also shown that the basaltic clinopyroxenes have boninitic affinity.

3.3. Post-Jurassic Strata

Following deposition of a thin sequence of basal red beds, variable thicknesses of Barremian to Albian, *Orbitolina*-bearing limestones overlie the Jurassic shales and slates [e.g., *Stöcklin*, 1968, *Braud*, 1990; *Agard et al*., 2005]. These carbonates form a conspicuous morphotectonic unit all along the SSA, especially along and near the MZT [*Huber*, 1977]. The carbonates form a series of parallel ridges formed by relatively mild, upright post-Cretaceous folding, with shearing along the contact between the competent limestones and its relatively incompetent substrate. The marine transgression is locally followed by Upper Cretaceous shales. Despite this shearing, it is clear in many areas that the sub-Cretaceous unconformity is sharply angular, in contrast to other unconformities in the sequence (Figure 2). The fact that the Jurassic sequence in the SSA is (1) intruded by Middle and Late Jurassic plutons and (2) locally metamorphosed (Figure 4), further contrasts the SSA with the nonvolcanic Jurassic-Cretaceous interval south of the MZT.

In the northwestern SSA, Cretaceous strata include abundant volcanics of diverse composition, from felsic to intermediate and mafic [e.g., *Eftekharnezhad*, 1973; *Azizi and Jahangiri*, 2008]. In the Sanandaj area, the volcanics occur within a thick sequence (>2000 m) of mostly shale deposits (Figure 5b) [*Stöcklin*, 1968; *Huber*, 1977]. Across the Iraqi border, in the Shalair zone, over 1000 m of mainly felsic volcanics overlie Albian orbitolina limestones [*Jassim and Goff*, 2006]. In Eqlid region (south of Abadeh) andesitic basalts occur as lavas and pyroclastics within Barremian-Cenomanian limestones (Figure 5f) [*Houshmandzadeh and Soheili*, 1990]. In the Sirjan-Hajiabad region extensive exposures of andesitic basalts and andesites with some dacites are interbedded with the Early Cretaceous limestones (Figure 5g) [*Sabzehei et al*., 1994; *Monsef et al*., 2011].

Table 1. Major Outcrops of Continental Metamorphic Complexes in the Sanandaj-Sirjan Zone, Listed From the Northwest to the Southeast

Complex Name	Structural Thickness (m)	Rock Types	Index Minerals	Protolith Age	Metamorphic/ Cooling Age
Khoy [*Khalatbari-Jafari et al.*, 2004] (Western complex)	>1000	Metaandesites, greenschists, and marble	Sericite, chlorite, and amphibole	Pre late Paleocene-early Eocene age	No data
Selvana and Serow [*Haghipour and Aghanabati*, 1988]	4000	Slates, phyllites, and felsic tuffs	Sericite and chlorite	Precambrian	1565 Ma (Rb-Sr) [*Haghipour and Aghanabati*, 1988]
Sursat and Takab region [*Alavi Naini et al.*, 1982; *Jamshidi Badr et al.*, 2010, 2012; *Kholghi Khasraghi*, 1999]	Intrusion Basal unit of a ~3000 m thick complex	Gneisses Micaschists	Hbl and biotite Garnet, staurolite, Al-silicates, and cordierite	540 ± 8 Ma [4]U-Pb zircon <605 ± 43 Ma [*Jamshidi Badr et al.*, 2010, 2012]U-Pb detrital zircon	61 ± 8 Ma (U-Th-Pb monazite) [*Jamshidi Badr et al.*, 2010, 2012]
Hamadan [*Mohajjel and Fergusson*, 2000; *Baharifar et al.*, 2004]	2000	Phyllites and micaschists	Garnet, staurolite, Al-silicates, and cordierite	Late Triassic-Early Jurassic	82 and 115 Ma (K-Ar amph) [*Baharifar et al.*, 2004]
June (Dorud-Azna) [*Mohajjel and Fergusson*, 2000]	2100	Schists, quartzites, Mg-marbles, metavolcanics, and gneisses	Sericite, chlorite, amphibole, epidote, and talc	Middle (± Late) Triassic?	No data
Chadegan, Zayandehrud [*Zahedi*, 1993; *Davoudian et al.*, 2007]	>1000	Amphibolites, gneisses, marbles, schists, and quartzites	Amphibole, micas, epidote, and garnet	Precambrian [*Zahedi*, 1993] Jurassic [*Davoudian et al.*, 2007]	172–184 Ma(Ar-Ar white mica) [*Davoudian et al.*, 2007]
Golpaygan [*Thiele et al.*, 1968; *Sheikholeslami and Zamani Pedram*, 2005; *Rachidnejad-Omran et al.*, 2002; *Moritz et al.*, 2006; *Hassanzadeh et al.*, 2008]	>2000	Micaschists, gneisses, marbles amphibolites, and quartzites	Garnet, staurolite, Al-silicates, and micas	Precambrian [*Thiele et al.*, 1968; *Hassanzadeh et al.*, 2008] Paleozoic [*Sheikholeslami and Zamani Pedram*, 2005; *Rachidnejad-Omran et al.*, 2002]	110 Ma (Ar-Ar amph), 87 Ma (Ar-Ar biot) [*Moritz et al.*, 2006] 151–174 Ma (K-Ar amph), 60–84 Ma (K-Ar biot) [*Rachidnejad-Omran et al.*, 2002]
Kolikosh (Heneshk-Gooshti) and Abadeh region [*Alric and Virlogeux*, 1977; *Houshmandzadeh and Soheili*, 1990]	>3500	Mg-Fe-marbles	Chlorite, biotite, garnet, amphibole, and epidote	Permian?	No data
Surian (Hassanabad) and Abadeh region [*Alric and Virlogeux*, 1977; *Houshmandzadeh and Soheili*, 1990]	Up to 1000	Schists, quartzites, marbles, and mafic metavolcanics	Garnet, chlorite, biotite, amphibole, and epidote	191 ± 12 Ma, U-Pb zircon [*Mousivand et al.*, 2012]	No data
Tootak (Kuh Sefid) + Bondono gneiss dome [*Alric and Virlogeux*, 1977; *Houshmandzadeh and Soheili*, 1990; *Hosseini et al.*, 2012; *Mousivand et al.*, 2012; *Alizadeh et al.*, 2010]	Intrusion	Orthogneiss	Biotite	514 ± 24 Ma, U-Pb zircon [*Hosseini et al.*, 2012]	73 Ma (Ar-Ar biot) [*Alizadeh et al.*, 2010]
	>4000	Marbles, graphite schists, and amphibolites	Garnet, biotite, epidote, hornblende, and talc	Silurian-Devonian [*Houshmandzadeh and Soheili*, 1990]	No data
Qori-Seghalton-Chah Dozdan and North of Neyriz [*Watters et al.*, 1970; *Sheikholeslami et al.*, 2008; *Fazlnia et al.*, 2007]	>1000	Amphibolites, marbles, metapelites, and gneisses	Hornblende, garnet, kyanite, sillimanite, staurolite, and biotite	Silurian-Carboniferous?	180 ± 21 Ma (U-Th-Pb monazite) [*Fazlnia et al.*, 2007] 87 Ma (Ar-Ar biot) [*Haynes and Reynolds*, 1980] 89, 170, and 184 Ma (K-Ar amph) [*Watters et al.*, 1970] 362 and 404 Ma (K-Ar biot)

AGU Tectonics

10.1002/2015TC003926

AGU Tectonics

10.1002/2015TC003926

Table 1. (continued)

Complex Name	Structural Thickness (m)	Rock Types	Index Minerals	Protolith Age	Metamorphic/ Cooling Age
					[*Watters et al.*, 1970] K-Ar amph peaks at 150 and 250 Ma [*Sheikholeslami et al.*, 2008] K-Ar biot peaks at 100 and 210 Ma [*Sheikholeslami et al.*, 2008]
Chah Gaz and NW Sirjan [*Mousivand et al.*, 2012]	Up to 500	Metarhyodacites, metabasalts, metapelites, and marbles	Sericite, chlorite	Paleozoic [*Watters et al.*, 1970] 174 ± 1.2 Ma [*Mousivand et al.*, 2012]	No data
South Sirjan and Godar-e Arabu [*Mijalkovic et al.*, 1972]	1600	Phyllites, calc-schists, and marbles	Biotite, chlorite, muscovite, and garnet	Permian	No data
	Unknown	Amphibolites and micaschists	Hornblende, biotite, garnet, and chlorite		
Hajiabad-Jiroft-Sirjan region [*Nazemzadeh et al.*, 1996; *Sabzehei*, 1974; *Sabzehei et al.*, 1994; *Ghasemi et al.*, 2002]					
Chah Choguk [*Nazemzadeh et al.*, 1996]	Up to 10,000	Slates, metasandstones, metadacites, metabasalts, and marbles	Sericite, chlorite, and actinolite	Late Paleozoic [*Nazemzadeh et al.*, 1996]	No data
Sargaz		Black slates, greenschists, and marbles	Hornblende, biotite, garnet, chlorite, and sericite	Devonian	325 Ma (K-Ar amph) 301 Ma (K-Ar biot)
Khabr		Marbles, calc-schists, and garnet schists			202 Ma (K-Ar amph) 199 Ma (K-Ar amph) [*Ghasemi et al.*, 2002]
Abshur		Amphibolites and marbles			
Rutchun		Metabasites, marbles, and calc-schists		Cambrian-Ordovician	No data
Gol-e Gohar-Barreh Koshan		Amphibolites, metabasites, gneisses, and anatectic granites			
Baghat		Metaultramafics and gneisses		Late Precambrian	
Bajgan and north Makran [*McCall*, 1985]	>1000	Phyllites, schists, marbles, quartzites, and amphibolites	Hornblende, actinolite, epidote, biotite, chlorite, and garnet	Paleozoic-Precambrian	Late Triassic and Senonian
Dur-Kan and north Makran [*McCall*, 1985]	>1000	Limestones, mafic to felsic lavas and dikes, and phyllites	Chlorite, muscovite, and epidote	Paleozoic-Mesozoic	Before the Late Valanginian [*Hunziker et al.*, 2015]

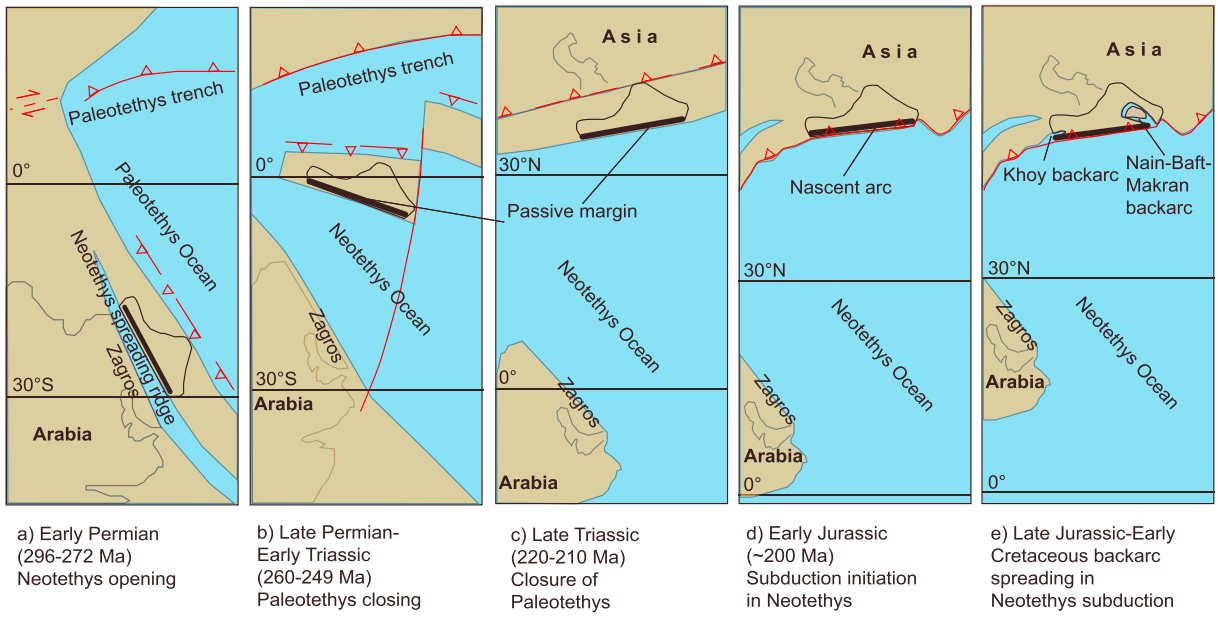

Figure 8. Diagrams showing evolution of Neotethys Ocean, from opening to subduction initiation, based on paleomagnetic data (simplified after *Stampfli and Borel* [2002] and *Muttoni et al.* [2009]).

The Cretaceous sequence is overlain in angular unconformity by widespread, polygenic, nonmarine conglomerates of assumed Paleocene age. The Paleocene deposits are succeeded by thin Eocene clastic-carbonate sequences, mostly along the margins of relatively sparse arc magmatic centers, although thicknesses of >1000 m in local half-grabens, such as the basins in the Golpaygan-Mahallat region, are attained [*Thiele et al.*, 1968; *Tillman et al.*, 1981; *Sheikholeslami and Zamani Pedram*, 2005; *Verdel et al.*, 2013]. However, in striking contrast to the adjoining Urumieh-Dokhtar arc in the northeast, the SSA is largely devoid of Tertiary volcanic rocks and plutons [*Stöcklin*, 1968]. The primary exception to this pattern is the basalts and andesites and their intrusive equivalents forming a limited arc parallel to the MZT between Sanandaj and the Iraqi border Iraq [*Leterrier*, 1985; *Azizi et al.*, 2011a; *Whitechurch et al.*, 2013] and extending northwestward into NE Iraq [*Ali et al.*, 2013]. These magmas represent only a minor component of the SSA, especially in comparison to the voluminous magmatism of this age in the Urumieh-Dokhtar arc.

The Tertiary stratigraphy of the SSA is dominated by reefal limestones of the Oligo-Miocene Qom Formation, which occur as scattered outcrops and for the most part are concentrated along topographic lows or depressions on the northeastern border zone of the belt (e.g., the Gavkhooni and Jazmurian depressions, Figure 1). Thicknesses are typically 100 m, but locally >1000 m. It overlies rocks ranging in age from late Proterozoic to Eocene with a distinct unconformity at the base [e.g., *Gansser*, 1955] and so delimits a major period of mid-Tertiary deformation, on a par with events that affected the region in Jura-Cretaceous time. The lower contact of the Qom Formation is diachronous. It is mostly early Miocene but may be as old as middle Oligocene in some areas [*Reuter et al.*, 2007]. Preservation around the border zone depressions is likely due to their subsidence although in the highs to the northwest of Jiroft a massive (~15 km by 15 km) outcrop unconformably overlies the deeply dissected Jurassic-Cretaceous volcano-sedimentary strata and the Jurassic Sargaz granite [*Timotijevic et al.*, 1972; *Chiu et al.*, 2013]. To the south of Sanandaj, in the northwestern segment of the arc, the Qom Formation and related deposits unconformably overlie Eocene marine strata and volcanics intruded by Eocene-Oligocene gabbros described further below [*Braud*, 1978; *Whitechurch et al.*, 2013]. Occurrences generally decline inward from the northern border zone but increase again toward the southern border (MZT), apparently reflecting the waning Tethyan trench during the Arabian collision.

Succeeding the Qom Formation, middle Miocene red beds and evaporates frequently occur around the border zone depressions, which are filled with younger mudstone and evaporites that form the modern playas. Younger volcanics, ranging in age from the Miocene to Quaternary, occur as lava domes and cinder cones between the towns of Qorveh and Takab in the northwestern part of the belt (Figure 3) [*Boccaletti et al.*, 1976; *Heidari*, 2014; *Heidari et al.*, 2015; *Allen et al.*, 2013].

4. Paleomagnetism and Permian-Triassic Drift History

During Late Paleozoic to Early Jurassic time, most of what is now Iran rifted away from Gondwanaland, shrinking the Paleotethys to the north and opening the Neotethys to the south, the latter now marked by a suture zone along the MZT [*Stöcklin*, 1974]. *Sengör* [1979] used the term "Cimmerian continent" for the continental fragments drifting in between the two Tethyan oceans. This fundamental idea was largely based on the occurrence of ophiolites of different age on either side of the Cimmerian blocks. The association of the Sanandaj-Sirjan zone with the *southern* margin of the Cimmerian continent in Jurassic time was originally based on the contrast in Mesozoic stratigraphy and structure across the MZT, as described above (Figure 2). This contrast was subsequently confirmed by paleomagnetic analysis of Late Paleozoic and Mesozoic strata in the Sanandaj-Sirjan zone and areas to the north in Iran, and their comparison with data from the Zagros Mountains, showing that the two regions were thousands of kilometers apart [*Soffel et al*., 1996; *Besse et al*., 1998; *Gallet et al*., 2000; *Muttoni et al*., 2009].

Neotethys seafloor spreading began between what are now the Zagros Mountains and the Sanandaj-Sirjan zone in the Permian, based on the formation of a passive margin preserved in the structural [*Navabpour et al*., 2010; *Tavakoli-Shirazi et al*., 2013], stratigraphic [*Berberian and King*, 1981], and igneous [*Berberian and Berberian*, 1981] records and on the aforementioned paleomagnetic data [*Besse et al*., 1998; *Muttoni et al*., 2009]. Paleoinclination data north of the Zagros suture record rapid northward movement of the Sanandaj-Sirjan zone and related areas (broadly, the Cimmerian subcontinent; Figure 8) from 270 to 220 Ma, when it shifted from African to Eurasian paleolatitude. Pre-270 Ma continental rifting is also suggested by a U-Pb zircon age of 288 Ma from a ferroan A-type granite 50 km east of Golpaygan in the central Sanandaj-Sirjan zone (Figures 3 and 4) [*Alirezaei and Hassanzadeh*, 2012]. As the Sanandaj-Sirjan zone pulled away from the Zagros (Africa-Arabia), carbonate platforms developed on both sides of the rift in Permian time. A massive carbonate and evaporite sequence, in excess of 2000 m thick, was deposited on the Zagros shelf [*Szabo and Kheradpir*, 1978]. At the same time, carbonates, shales, sandstones and, locally, volcanics were deposited in the Sanandaj-Sirjan zone. As alluded to above, they attained thicknesses of up to 3500 m and are among the few sections worldwide that conformably span the Permo-Triassic boundary [e.g., *Heydari et al*., 2003]. In contrast, in the Zagros Mountains, a substantial unconformity separates Permian and Triassic strata (Figure 2) [e.g., *Szabo and Kheradpir*, 1978]. In the Abadeh section, an Artinskian (Early Permian) marine fauna at the base of the synrift section and subsequent carbonate platform deposition through the remainder of the Permian [*Taraz*, 1974] suggest that the onset of the "drift" or seafloor spreading phase in the Neotethys Ocean occurred near the end of Artinskian time, or about 276 Ma.

In summary, these data indicate that by Late Triassic time (circa 220 Ma), the Alborz Mountains, Central Iran, and Sanandaj-Sirjan zone were close to the Eurasian margin, and about 30° north of Arabia, thus placing the main Neotethyan suture south of the SSA (Figure 8).

5. Metamorphism

It has long been noted that the Iranian collision zone does not contain an extensive, continuously exposed internal zone or "core" of collision-related metamorphic rocks [*Stöcklin*, 1968; *Berberian and King*, 1981; *Mohajjel and Fergusson*, 2014], in contrast to much of the Alpine-Himalayan collision zone (and collisional orogens in general, e.g., the Pennine zone in the western Alps, the Vardar-Cyclades-Menderes metamorphic core zone of the Aegean region, or the Blue Ridge province of the southern Appalachians). The Sanandaj-Sirjan zone is perhaps the closest analog, generally regarded as the most internal, metamorphic core of the broader Asian collision zone [e.g., *Yin*, 2010] at the longitude of Iran. But the distribution of metamorphic rocks is relatively sparse and discontinuous, and as outlined below, much of the metamorphism predates the Arabia-Asia collision by 100 Myr or more.

Detailed understanding of the metamorphic history is accordingly fragmentary and appears to vary markedly between various isolated exposures of metamorphic rocks. Data pertaining to the metamorphic history within each of 16 major exposures of metamorphic rocks are summarized in Table 1, from northwest to southeast. These data indicate that the metamorphic history of the SSA is protracted, complex, and probably occurred in multiple phases. In most areas, both the protolith ages and the timing of recrystallization events are poorly constrained owing to a lack of radiometric data. For instance, *Berberian et al*. [1981] proposed up to

four metamorphic episodes in the Aligoodarz-Golpaygan region (Figure 3) including the following: Late Precambrian (amphibolite facies), Hercynian (greenschist), Middle Triassic (zeolite), and Late Jurassic-Late Cretaceous (low greenschist). Also, three distinct metamorphic events, ranging from high to low grades, have been suggested for pre-Cretaceous rocks in the area between Sirjan and Hajiabad in the southeastern part of the SSA [*Berberian*, 1977]. However, metamorphic age assignments are speculative due to sparse geochronological constraints, emphasizing a need for petrofabric studies supplemented by in situ compositional analysis and dating.

The Paleozoic-Jurassic sedimentary and volcanic succession generally displays subgreenschist to low greenschist facies metamorphism (e.g., the Hamadan phyllites). To first order, they are deformed by NW trending (orogen-parallel) flexural-slip folding and thrust faulting and are overlain in angular unconformity by unmetamorphosed Cretaceous Orbitolina-bearing limestones, similar to those exposed throughout Central Iran [e.g., *Stöcklin*, 1968; *Agard et al*., 2005].

The volumetrically most significant exposures of low- to medium-grade metamorphism of demonstrably Jurassic sedimentary and volcanic strata occur to the east of the Jurassic batholith in the Hamadan area (Hamadan phyllites and related rocks). Metamorphism is restricted to the Buchan (or Abukuma) facies series (andalusite, sillimanite, and cordierite, among other high-temperature phases) [e.g., *Baharifar et al*., 2004; *Agard et al*., 2005; *Sepahi et al*., 2009; *Shahbazi et al*., 2010]. The high-*T*, low-*P* metamorphic conditions in this region have locally triggered migmatization [e.g., *Sepahi et al*., 2009]. From the petrogenesis of quartz-rich andalusite-kyanite-sillimanite veins that crosscut metapelites, pressure-temperature (*P-T*) paths indicate that pressure and temperature conditions appear not to have significantly exceeded the aluminum silicate triple point, i.e., 500°C and 4 kbar [*Sepahi et al*., 2004].

Much younger Barrovian-type metamorphism has been identified within three isolated, areally restricted exposures in the northwest, central, and southeastern part of the SSA, at least some of which appear to have been exhumed within Cordilleran-type metamorphic core complexes of Cretaceous (?)-Paleogene age [e.g., *Stockli et al*., 2004; *Verdel et al*., 2007; *Hassanzadeh et al*., 2008]. In the northwest, the Sursat complex to the west of Takab (Table 1 and Figure 4) consists of two-mica metapelites containing garnet, staurolite, kyanite, sillimanite, andalusite, cordierite, and actinolite, intruded by premetamorphic Pan-African granites yielding U-Pb ages circa 540 Ma [*Jamshidi Badr et al*., 2012]. Protoliths of this complex were first assigned to the Precambrian [*Alavi Naini et al*., 1982], now supported by a U-Pb detrital zircon study of a staurolite schist that yielded a maximum depositional age of 605 ± 43 Ma for the protolith [*Jamshidi Badr et al*., 2010]. The same study suggests that regional metamorphism took place at 61 ± 8 Ma based on the U-Pb dating of monazite from garnet schists. The timing of monazite crystallization in these metapelites is coeval with the emplacement of the Paleocene batholiths in the same vicinity [*Kholghi Khasraghi*, 1999; *Jamshidi Badr et al*., 2012; *Heidari*, 2014].

In the central SSA, north and northeast of Golpaygan, dominantly sedimentary protoliths of uncertain age now containing garnet, staurolite, kyanite, and sillimanite occur in the footwalls of Tertiary detachment faults [e.g., *Moritz et al*., 2006; *Verdel et al*., 2007, 2013]. Because these regional metamorphic rocks are found in proximity to subgreenschist Paleozoic strata as old as Cambrian, their protoliths have tentatively been assigned a Precambrian age [e.g., *Thiele et al*., 1968]. However, *Rachidnejad-Omran et al*. [2002] have called for a Palaeozoic protolith age based on uncertain fossil evidence and lithostratigraphic correlation with unmetamorphosed volcanosedimentary sequences in Central Iran. The Precambrian age assignment of the protoliths, at least in part, was confirmed by Pan-African ages obtained from granitic gneisses that intrude them [*Hassanzadeh et al*., 2008]. K-Ar amphibole ages of circa 180 to 150 Ma [*Rachidnejad-Omran et al*., 2002] suggest that metamorphism was predominantly Jurassic. A more complete set of cooling ages, including Ar-Ar amphibole and mica ages [*Moritz et al*., 2006] and (U-Th)/He dating of apatite and zircon [*Verdel et al*., 2013] suggest that cooling from amphibolite facies conditions was underway by Early Cretaceous time for at least parts of the complex (~110 Ma). However, tectonite fabrics are present in granitoids in the complex that have crystallization ages as young as Paleogene (circa 63 Ma), and cooling ages are as young as middle Eocene (circa 50–55 Ma) [*Verdel et al*., 2013].

In the southeastern SSA, Barrovian-type assemblages are extensively exposed in highlands in the Neyriz-Sirjan-Hajiabad region that extend eastward to Jiroft (Figure 3) [*Sabzehei et al*., 1994]. The complex consists of amphibolites, metapelites, metabsites, marbles, and gneisses, tectonically juxtaposed with Buchan-type assemblages of likely Jurassic age [*Watters et al*., 1970; *Haynes and Reynolds*, 1980; *Sabzehei et al*., 1994;

Sheikholeslami et al., 2008; *Fazlnia et al*., 2013]. Protolith and metamorphic ages are, however, controversial (Table 1). Some of the metamorphic rocks may be unconformably overlain by Jurassic volcanosedimentary deposits, above a basal conglomerate that putatively contains detrital Al-silicate grains [*Watters et al*., 1970]. Other parts of the complex yield Late Paleozoic K-Ar ages. These observations have led to the conclusion that the protoliths may include strata as young as Late Paleozoic and that the Barrovian-type metamorphism is of Triassic age [*Watters et al*., 1970; *Berberian and King*, 1981; *Sabzehei et al*., 1994]. However, the conglomerate itself is metamorphosed (neoform chlorite and epidote) [*Watters et al*., 1970], raising the possibility that most of the metamorphism postdates the Jurassic volcanosedimentary deposits. Further, an orthogneiss within the metamorphic package yielded a 520 Ma U-Pb zircon age, suggesting that the protolith country rock is Lower Cambrian or older [*Sheikholeslami et al*., 2008]. Therefore, as is the case at Golpaygan, the protolith age of these high-*T*-*P* rocks could be entirely Precambrian [e.g., *Stöcklin*, 1968] (Table 1), overprinted by Jurassic or younger metamorphic events. More recent relevant observations in the region include the following: (1) low-pressure felsic metavolcanic rocks that occur along the fault-bounded northern margin of the complex contain middle Jurassic magmatic zircons [*Mousivand et al*., 2011] (Table 1); (2) Buchan-type metamorphism is spatially associated with the large Chah Dozdan and Siahkuh Jurassic batholiths (Table 3) [*Fazlnia et al*., 2007, 2009, 2013]; and (3) metapelite xenoliths in the Chah Dozdan batholith yielded a U-Th-total Pb monazite age of 180 ± 21 Ma [*Fazlnia et al*., 2007]. These data may be most simply explained by a high-*T* metamorphic event of Jurassic age, in contrast to the more complex three-event history inferred from clusters of K-Ar ages by *Sheikholeslami et al*. [2008] (mid-Triassic, Early Jurassic, and Late Cretaceous). Farther SE, various schists of unknown protolith age lie unconformably (?) beneath Jurassic strata to the west of Jiroft [e.g., *Dimitrijevic*, 1973].

Exposures of high-*P*, low-*T* rocks are even more localized. Blueschist facies rocks are preserved in tectonic slivers underplating the SSA along the MZT zone south of Sirjan, in association with regional colored mélange [*Haynes and Reynolds*, 1980; *Berberian and King*, 1981]. Ar-Ar phengite ages of 85–95 Ma suggest when these rocks cooled below 375°C by exhumation in the subduction channel and that this event broadly coincides with Cretaceous colored mélange accretion in the overriding plate of the present-day collisional setting [*Agard et al*., 2006]. It is noteworthy that this is the only documented example of an accretionary complex related to the subduction at the southern margin of the SSA. The juxtaposition of blueschist facies rocks in the south Sirjan-Hajiabad region at the rear of the Zagros suture with the Barrovian- and Buchan-type assemblages farther north in the Neyriz-Sirjan area is reminiscent of the Sanbagawa-Abukuma paired metamorphic belt of Japan [e.g., *Miyashiro*, 1973], although the Barrovian-type assemblages are more pronounced in the case of the southeastern SSA.

Within exposures of Barrovian-series metamorphic rock in the central SSA west of Esfahan (Figure 4), selvages of eclogite facies rocks that yield middle Jurassic white mica cooling ages were discovered within one of these metamorphic complexes [*Davoudian et al*., 2007]. These ages have led to a new hypothesis that an arc-parallel oceanic basin was present within the SSA in the Jurassic [*Davoudian et al*., 2007; *Arfania and Shahriari*, 2009]. However, parts of the same crystalline terrain appear to be nonconformably overlain by unmetamorphosed Jurassic strata less than 10 km away [*Zahedi*, 1993], and the age of both protoliths and eclogite-facies metamorphism is unconstrained.

6. Plutonism

For the first time, crystallization ages for intrusive rocks have become widely available over the last decade, allowing a much more detailed depiction of the "tectonoplutonic episodes" of the zone originally proposed in the pioneering paper by *Berberian and Berberian* [1981]. In general, magmatism provides an independent window into the development of its cratonic basement, the Neotethyan passive margin, and the subsequent conversion from passive margin to subduction zone in Early Mesozoic time. Plutonic activity in the SSA spans at least half a billion years and has been highly variable in composition, time, and space. Despite this long and complex history, the most dominant episode is the Jurassic event that forms the SSA.

We have compiled the basic age and compositional data on >60 plutonic centers, which range in age from late Proterozoic to late Miocene (Tables 2 and 3 and Figures 3, 7, and 9). Histograms of the distribution of ages indicate five principal plutonic episodes, at (1) late Proterozoic-Cambrian, (2) Late Carboniferous-Early Permian, (3) Early and Middle Jurassic (volumetrically the most important event, with a conspicuous

Table 2. Major Plutons of the Sanandaj-Sirjan Zone, Listed From the Northwest to the Southeast

			Age		
Age Group	Pluton	Rock Type	Stratigraphic	Crystallization (U-Pb Zircon, Ma)	Cooling[a] (Ma)
Miocene	Touzlar and Takab	Microdioritr porphyry	Neogene	18 ± 0.2, 19 ± 0.3 [*Heidari et al.*, 2015]	No data
	Sari Gunay and Qorveh	Trachydacite porphyry	Neogene	No data	11–12 (Ar-Ar) [*Richards et al.*, 2006]
Eocene	Piranshahr	Granite, pulaskite, and gabbro	Late Cretaceous-Paleocene	41 ± 0.2 [*Mazhari et al.*, 2009]	No data
	Naqadeh	Monzogranite and diorite	Late Cretaceous-Paleocene	41 ± 2, 42 ± 1 [*Mazhari et al.*, 2011a; *Mazhari et al.*, 2011b]	No data
	Marivan, Sanandaj	Granodiorite and quartzdiorite	Late Eocene-Early Oligocene	38 ± 2 [*Sepahi et al.*, 2014]	No data
	Sursat Mountain and Takab	Syenogranite	Late Cretaceous-Paleocene	55 ± 2 [*Jamshidi Badr et al.*, 2010]	No data
	Taa-Baysaran, Kamyaran, and Sanandaj	Gabbro and diorite	Post Middle Eocene	35 ± 4, 37 ± 0.5 [*Azizi et al.*, 2011a]	38–40 K-Ar [*Braud*, 1990] 27 K-Ar biot [*Whitechurch et al.*, 2013] 34 Rb-Sr [*Leterrier*, 1985]
	Gamasiab and Harsin	Diorite	Post Paleocene	No data	59 K-Ar amph [*Whitechurch et al.*, 2013]
	Goosheh-Tavandasht	Quartzmonzodiorite	Post Jurassic	35 ± 0.1 [*Mahmoudi et al.*, 2011]	No data
Paleocene	Ghushchi and NW Lake Urumieh [*Khodabandeh and Amini-Fazl*, 1993]	Biotite granite, diorite, and gabbro	Late Cretaceous-Paleocene	No data	No data
	Serow [*Haghipour and Aghanabati*, 1988]	Porphyritic biotite granite	Late Cretaceous-Eocene	No data	No data
	Baneh, Marivan, and W. Sanandaj [*Fonoudi and Sadeghi*, 2003]	Granite and diorite	Late Cretaceous-Paleocene	No data	No data
	Bukan Dam and Takab	Quartzmonzonite	Late Cretaceous-Paleocene	No data	97 K-Ar biot [*Kholghi Khasraghi*, 1999]
	Pichaghchi-Turke Dare and Sursat Mountain	Granodiorite	Late Cretaceous-Paleocene	56 ± 2, 59 ± 3 [*Jamshidi Badr et al.*, 2010]	75 K-Ar biot [*Jamshidi Badr et al.*, 2010]
	Gozal Bolagh and Shahindezh	Granodiorite	Late Cretaceous-Paleocene	60 ± 1 [*Heidari*, 2014]	No data
	Hassan Salari-Lakzy Dam	Granite	Late Cretaceous-Paleocene	60 ± 0.2 [*Mahmoudi et al.*, 2011]	No data
Cretaceous	Urumieh-Oshnavieh [*Ghalamghash et al.*, 2009a, 2009b]	Diorite, granite, and syenite Nari biotite granite	Late Cretaceous-Paleocene	No data	76–100 K-Ar 99 K-Ar
	Naqadeh	Diorite and gabbro	Late Cretaceous-Paleocene	97 ± 2 [*Mazhari et al.*, 2011b]	No data
	Hassan Salari and Saqqez	Leucogranite	Late Cretaceous-Paleocene	109 ± 0.3 [*Mahmoudi et al.*, 2011]	No data
	Sufiabad and Qorveh	Leucogranite Gabbro, monzonite, and granite	Late Jurassic Late Jurassic	144 ± 2 [*Azizi et al.*, 2011b] No data	No data

AGU Tectonics

10.1002/2015TC003926

Table 2. (continued)

Age Group	Pluton	Rock Type	Age		
			Stratigraphic	Crystallization (U-Pb Zircon, Ma)	Cooling[a] (Ma)
	Mobarakabad and Qorveh [*Azizi and Asahara*, 2013]				131 ± 27 Rb-Sr 185 ± 45 Rb-Sr 188 ± 62 Rb-Sr
	Almogholagh, Asadabad, and Hamadan	Diorite and syenite	Post Jurassic	No data	144 ± 17 Rb-Sr [*Valizadeh and Zarian*, 1976]
	Cheshmeh Sefid-Esfajerd (Golpaygan)	Syenite, diorite, and gabbro	Precambrian [*Thiele et al.*, 1968], Post Early Cretaceous [*Sheikholeslami and Zamani Pedram*, 2005]	No data	55 Ar-Ar amph-biot [*Moritz et al.*, 2006]
Jurassic: See Table 3					
Triassic?	Mazar (Bagh Kenar-Deh Sard, Khabr)	Trondhjemite, granodiorite, and gabbro	Late Triassic [*Nazemzadeh et al.*, 1997; *Sabzehei et al.*, 1994] Post Late Cretaceous [*Nazemzadeh and Rashidi*, 2007]	No data	No data
Late Carboniferous-Early Permian	Ghushchi and NW Lake Urumieh [*Khodabandeh and Amini-Fazl*, 1993]	Gabbro and granite	Precambrian, Pre-Permian	320 ± 2.5 [*Shafaii Moghadam et al.*, 2015]	No data
	Khalifan and south Lake Urumieh	Flourite leucogranite	Late Cretaceous-Paleocene	315 ± 2 [*Bea et al.*, 2011]	277 ± 5 Rb-Sr [*Bea et al.*, 2011]
	Darehadavand and Azna	Metagabbro		315 ± 4 [*Alizadeh et al.*, 2010]	
	Hasan Robat	Biot-hbl granite	Precambrian [*Thiele et al.*, 1968]	288 ± 4 [*Alirezaei and Hassanzadeh*, 2012]	No data
	Sikhoran	Anatectic granite	Pre Late Permian	No data	330 K-Ar [*Ghasemi et al.*, 2002]
Cambrian-Ordovician	South Sirjan [*Roshan Ravan et al.*, 1997]	Gneissose granite	Post Permian-pre Late Jurassic [*Mijalkovic et al.*, 1972]	No data	No data
Late Proterozoic-Cambrian	Gushchi and NW Lake Urumieh	Gneissose granite	Precambrian [*Khodabandeh and Amini-Fazl*, 1993]	571 ± 5 [*Shafaii Moghadam et al.*, 2015]	No data
	Sheikh Chupan and Saqqez	Biot-hbl granodiorite porphyry	Early Cambrian [*Eftekharnezhad*, 1973]Post Cretaceous [*Omrani and Khabbaznia*, 2003]	551 ± 25 [*Hassanzadeh et al.*, 2008]	No data
	Bubaktan and Saqqez	Biotite quartzmonzonite	Early Cambrian [*Eftekharnezhad*, 1973]Post Cretaceous [*Omrani and Khabbaznia*, 2003]	544 ± 19 [*Hassanzadeh et al.*, 2008]	No data
	Sursat and Takab	Augen gneiss and syenogranite	Early Cambrian [*Eftekharnezhad*, 1973]	543 ± 6, 537 ± 8 [*Jamshidi Badr et al.*, 2010]	No data
	Galeh Doz (June complex) and Azna	Orthogneiss-granite	Triassic [*Mohajjel and Fergusson*, 2000]	588 ± 41 [*Shakerardakani et al.*, 2015]608 ± 18 [*Shakerardakani et al.*, 2015] 568 ± 11 [*Nutman et al.*, 2014]	No data
	Chadegan and Zayandehrud Dam	Orthogneiss-granite	Precambrian	630 ± 20, 586 ± 26 [*Nutman et al.*, 2014]	Ar-Ar ~110–170 [*Davoudian et al.*, 2007]

AGU Tectonics

10.1002/2015TC003926

AGU Tectonics

10.1002/2015TC003926

Table 2. (continued)

Age Group	Pluton	Rock Type	Age		
			Stratigraphic	Crystallization (U-Pb Zircon, Ma)	Cooling[a] (Ma)
	North Varzaneh and Golpaygan	Biotite orthogneiss	Precambrian [*Thiele et al.*, 1968] Paleozoic [*Rachidnejad-Omran et al.*, 2002]	588 ± 23 [*Hassanzadeh et al.*, 2008]	60 K-Ar biot [*Mijalkovic et al.*, 1972]
	Muteh, Chah Khatoon, and Golpaygan	Biotite granite and leucogranite	Precambrian [*Thiele et al.*, 1968] Paleozoic [*Rachidnejad-Omran et al.*, 2002]	578 ± 22,596 ± 24 [*Hassanzadeh et al.*, 2008]	73 Ar-Ar biot [*Moritz et al.*, 2006]68 K-Ar biot [*Rachidnejad-Omran et al.*, 2002]
	Bondono, Tutak, and East of Abadeh	Biotite orthogneiss	Paleozoic [*Alric and Virlogeux*, 1977; *Houshmandzadeh and Soheili*, 1990]	514 ± 24 [*Hosseini et al.*, 2012]	73 Ar-Ar biot [*Alizadeh et al.*, 2010]
	Kor-e Sefid(Qori metamorphic complex), East of Abadeh	Biotite orthogneiss	Paleozoic [*Houshmandzadeh and Soheili*, 1990]	520 [*Sheikholeslami et al.*, 2008]	K-Ar amph peaks at 150 and 250 Ma [*Sheikholeslami et al.*, 2008]K-Ar biot peaks at 100 and 210 Ma [*Sheikholeslami et al.*, 2008]
	Sikhoran, SE of Sirjan	Layered gabbros and peridotites	Late Precambrian-Early Paleozoic [*Sabzehei et al.*, 1994]	No data	253 and 256 K-Ar amph [*Ghasemi et al.*, 2002]

[a]Some of the dates in this column are older than the crystallization ages due to excess argon (K-Ar dates) or large error margins (Sm-Nd and Rb-Sr dates).

Table 3. Major Jurassic Plutons of the Sanandaj-Sirjan Arc, Listed From the Northwest to the Southeast

Pluton	Rock Type	Age		
		Stratigraphic	Crystallization (U-Pb zircon, Ma)	Cooling[a] (Ma)
Sufiabad, Qorveh	Granite and diorite	Late Jurassic	148 ± 1, 149 ± 2 [*Azizi et al.*, 2011b] 157 ± 1 [*Mahmoudi et al.*, 2011]	No data
Mayham, Qorveh	MonzoniteGabbro	Late Jurassic	151 ± 0.2 [*Mahmoudi et al.*, 2011] 149 ± 0.2 [*Mahmoudi et al.*, 2011]	No data
Hamadan (Alvand batholith)	Porphyritic granite Diorite Leucogranite and granite Leucogranite Microgranite Gabbro Pegmatite	Late Jurassic	165 ± 0.2 [*Mahmoudi et al.*, 2011] 165 ± 0.4 [*Mahmoudi et al.*, 2011] 164 ± 2 and 165 ± 2 [*Chiu et al.*, 2013] 154 ± 1 [*Shahbazi et al.*, 2010] 162 ± 5 [*Shahbazi et al.*, 2010] 167 ± 0.2 [*Shahbazi et al.*, 2010] No data	61–65 K-Ar biot [*Braud*, 1990] 82 K-Ar biot [*Baharifar et al.*, 2004] 65 and 200 Rb-Sr biot [*Valizadeh and Cantagrel*, 1975] 62–102 K-Ar biot [*Valizadeh and Cantagrel*, 1975] 79 and 89 Rb-Sr biot [*Valizadeh and Cantagrel*, 1975] 89 K-Ar biot [*Valizadeh and Cantagrel*, 1975] 104 Rb-Sr musc [*Valizadeh and Cantagrel*, 1975] 83 K-Ar musc [*Valizadeh and Cantagrel*, 1975]
Malayer	Granite, tonalite, granodiorite, and syenogranite	Late Jurassic	162 ± 0.7 to 187 ± 0.3 [*Ahadnejad et al.*, 2011]	No data
Boroujerd	Quartzdiorite, granodiorite, and monzogranite Pegmatite	Late Jurassic Late Jurassic	170 ± 0.2 to 172 ± 1.5 [*Ahmadi-Khalaji et al.*, 2007] No data	62–130 Rb-Sr micas [*Masoudi et al.*, 2002] 119–127 Rb-Sr [*Masoudi et al.*, 2002]
Nezamabad	Monzogranite	Late Jurassic	170 ± 0.3 [*Mahmoudi et al.*, 2011]	No data
Astaneh-Shazand	Granite	Late Jurassic	168 ± 1 [*Mahmoudi et al.*, 2011]	99 Rb-Sr [*Masoudi et al.*, 2002]
June, north Azna	Granitic gneiss	Late Jurassic [*Sahandi et al.*, 2006]	No data	No data
Darijune, north Azna	Gabbro	Post Late Triassic-Early Jurassic [*Sahandi et al.*, 2006]	170 ± 3 [*Shakerardakani et al.*, 2015]	No data
Chadegan, Zayandeh-Rud River	Granitic gneiss	Precambrian [*Zahedi*, 1993] Middle Jurassic [*Ghasemi et al.*, 2006]	No data	175 Ar-Ar phengite [*Davoudian et al.*, 2007]
Aligoodarz	Granite	Late Jurassic	165 ± 5 [*Esna-Ashari et al.*, 2012]	No data
Khansar, South of Golpaygan	Granodiorite, granite, and diorite	Late Jurassic-Early Cretaceous [*Thiele et al.*, 1968]	No data	No data
Kolah Ghazi, S of Esfahan	Granite	Late Jurassic	165 ± 2 [*Chiu et al.*, 2013]	No data
Jian, Bavanat	Granite	Late Jurassic [*Shahidi*, 2000]	No data	No data
Tootak, Bavanat	Aplite granite	Pre-Permian	173 ± 9 [*Hosseini et al.*, 2012]	177 Ar-Ar musc [*Alizadeh et al.*, 2010]
Qori, Neyriz	Trondhjemite	Mesozoic	147 ± 1 [*Fazlnia et al.*, 2009]	No data
Chah Dozdan- Chah Bazargan	Anorthosite, quartzdiorite, granite, and gabbro	Mesozoic and Triassic [*Watters et al.*, 1970]	171 ± 2, 173 ± 2, and 164 ± 8 [*Fazlnia et al.*, 2007; *Fazlnia et al.*, 2013]	118 K-Ar musc and 164 K-Ar biot [*Watters et al.*, 1970] 118 K-Ar musc, 152 K-Ar biot, and 162 K-Ar biot [*Watters et al.*, 1970]
Kuh-e Khaju, South Sirjan	Foliated biotite granite	Cambrian-Ordovician [*Roshan Ravan et al.*, 1997]Jurassic [*Dimitrijevic*, 1973]	No data	No data
Siahkuh, west Jiroft	Granodiorites, monzogranites, granites, and gabbros	Late Triassic [*Sabzehei et al.*, 1994] Middle Jurassic [*Timotijevic et al.*, 1972] Post Late	No data	199 ± 30 Sm-Nd [*Arvin et al.*, 2007]

AGU Tectonics

10.1002/2015TC003926

Table 3. (continued)

Pluton	Rock Type	Age		
		Stratigraphic	Crystallization (U-Pb zircon, Ma)	Cooling[a] (Ma)
Sikhoran	Gabbro	Cretaceous [*Nazemzadeh and Rashidi*, 2007] Late Triassic-Early Jurassic [*Sabzehei et al.*, 1994]	No data	220 K-Ar amph [*Ghasemi et al.*, 2002]
Sargaz, NW Jiroft	Granite	Middle Jurassic	175 ± 2 [*Chiu et al.*, 2013]	No data
Remeshk-Ramak (Fannuj, north Makran)	GraniteDiorite, trondhjemite, and plagiogranite	Pre Cretaceous-Paleocene [*McCall*, 1985]	170 ± 1 to 176 ± 1 [*Hunziker et al.*, 2015]153 ± 1 to 166 ± 1 [*Hunziker et al.*, 2015]	140–133 [*Hunziker et al.*, 2015]

[a]Some of the dates in this column are older than the crystallization ages due to excess argon (K-Ar and Ar-Ar dates) or large error margins (Sm-Nd and Rb-Sr dates).

maximum at ~170 Ma), (4) Cretaceous-Paleogene in the northwestern SSA (which appears to be a continuation of the Jurassic event), and (5) Miocene subvolcanic porphyries of the Qorveh-Takab region (Tables 2 and 3 and Figure 9). As noted in section 3, there are locally significant mafic and bimodal volcanics within Late Triassic strata, but as yet there are no known plutons or radiometric ages from this magmatic event.

6.1. Pre-Jurassic Plutons

The SSA includes numerous Pan-African-type late Proterozoic-Early Cambrian calc-alkaline granitoids, with published crystallization ages ranging from circa 630 to 514 Ma. The peak of activity occurred in the 560 to 540 Ma range [e.g., *Hassanzadeh et al.*, 2008; *Sheikholeslami et al.*, 2008; *Azizi et al.*, 2011c; *Jamshidi Badr et al.*, 2012; *Hosseini et al.*, 2012; *Nutman et al.*, 2014; *Shakerardakani et al.*, 2015]. From a magmatic perspective, the prearc crystalline basement of the SSA exhibits similarity with Central Iran and the rest of the country, except for the Kopet Dagh belt of the pre-Norian Eurasian margin in NE Iran (Figure 1), which does not expose any Pan-African rocks. More intrusives with Pan-African ages will likely be revealed by ongoing dating efforts. Inherited zircons of this age are ubiquitous in many of the younger plutons, signaling the presence of basement rocks with Arabian affinity in the subsurface that are considerably more extensive than surface outcrops would suggest (Figures 3 and 9b) [e.g., *Mazhari et al.*, 2011a, 2011b; *Chiu et al.*, 2013]. Whereas all of the major tectonic components (except for the ophiolites) of Iran contains exposures of Pan-African crystalline rocks, the succeeding plutonic episodes in Late Carboniferous-Early Permian and Jurassic time appear to be restricted to the SSA, markedly distinguishing it from the other components.

The subsequent Late Carboniferous- Early Permian event is relatively sparsely exposed, consisting of only four plutonic centers known thus far. In the central SSA, the Hasan Robat pluton, 50 km east of Golpaygan, yielded a U-Pb zircon age of 288 Ma and is a ferroan A-type rift-related granite [*Alirezaei and Hassanzadeh*, 2012]. The second example is the NW Azna metagabbro at about 100 km west of Golpaygan with U-Pb zircon age of circa 315 Ma (Figure 3) [*Shakerardakani et al.*, 2015]. In the NW part of the SSA, about 1000 km NW of Golpaygan near Mahabad, a fluorite-bearing A-type granite has a U-Pb zircon age of 314 Ma [*Bea et al.*, 2011]. A fourth example of A-type granitoids occurs still farther NW, about 70 km north of Urumieh, and yields a U-Pb zircon age of circa 320 Ma [*Shafaii Moghadam et al.*, 2015] (Table 2 and Figure 3). As noted above, plutonic suites with later Permian or Triassic crystallization ages have not yet been reported, but inherited zircons with this age range occur within the Jurassic granitoids, suggesting that there may be unexposed igneous bodies of that age at depth [*Shahbazi et al.*, 2010; *Ahadnejad et al.*, 2011; *Mahmoudi et al.*, 2011; *Esna-Ashari et al.*, 2012; *Chiu et al.*, 2013] (Figure 9b).

6.2. Jurassic Plutons

In contrast to the limited exposures of any plutons of Middle Cambrian through Triassic age, Jurassic intrusives are ubiquitous,

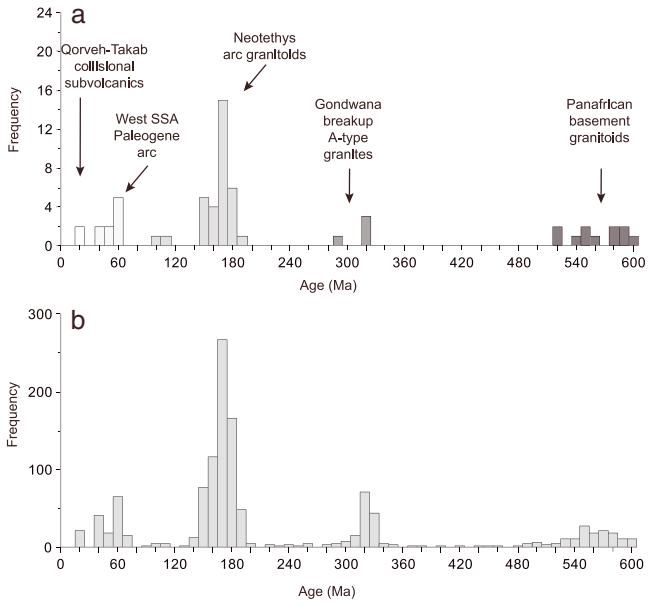

Figure 9. Frequency histogram of U-Pb zircon ages compiled from the literature cited in the text. (a) Ages of igneous intrusion, showing five distinct groups including basement Pan-African arc granitoids, Late Carboniferous-Early Permian rift-related "A-type" granites, Jurassic-Cretaceous Neotethyan arc batholiths, Late Cretaceous-Paleogene arc magmas, and Neogene collisional subvolcanic intrusives. (b) Ages of >1100 individual grains, including inherited zircons, which enhance peaks of the mostly buried Pan-African and Late Carboniferous-Early Permian plutons.

with reliable crystallization ages as old as circa 187 Ma, and a pronounced age peak near 170 Ma (Figures 7 and 9 and Table 3). Typically intruding Jurassic volcanosedimentary strata, the SSA plutonic core comprises a 30 to 50 km wide belt of irregularly spaced granitoid stocks and batholiths (Figure 7), variably accompanied by smaller volume diorites, gabbros, and locally, pyroxenite cumulates (Table 3). Owing to deuteric alteration, arc plutonism has been more extensively studied than the volcanics, and therefore, a relatively rich age and geochemical database is emerging for the SSA granitoids. Data on 22 plutonic centers with definite or likely Jurassic ages are assembled in Table 3. A broad range of K-Ar and Rb-Sr cooling ages, mostly ranging from Cretaceous to Paleocene, had previously been assumed to be crystallization ages for a number of these plutonic centers [e.g., *Valizadeh and Cantagrel*, 1975; *Berberian and Berberian*, 1981; *Braud*, 1990], but U-Pb zircon ages published over the last decade show that the plutons dated thus far were emplaced almost entirely during Jurassic to Early Cretaceous time (circa 187 to 97 Ma) [*Ahmadi-Khalaji et al.*, 2007; *Fazlnia et al.*, 2007, 2009, 2013; *Shahbazi et al.*, 2010; *Ahadnejad et al.*, 2011; *Mahmoudi et al.*, 2011; *Azizi et al.*, 2011b; *Esna-Ashari et al.*, 2012; *Hosseini et al.*, 2012; *Chiu et al.*, 2013; *Hunziker et al.*, 2015]. Whole-rock major and trace element compositions of many of these plutons have been presented in a number of recent publications and reveal calc-alkaline affinity and arc-related geochemical signatures [*Arvin et al.*, 2007; *Ahmadi-Khalaji et al.*, 2007; *Fazlnia et al.*, 2009, 2013; *Shahbazi et al.*, 2010; *Ahadnejad et al.*, 2011; *Mahmoudi et al.*, 2011; *Esna-Ashari et al.*, 2012; *Hunziker et al.*, 2015]. While the majority of the granitoids are I-type, some A-type examples have been identified throughout the zone [e.g., *Sarjoughian et al.*, 2015, and references therein]. The more deeply eroded plutonic systems (e.g., in the Alvand batholith in the Hamadan region and the Aligoodarz batholith) expose mafic bodies of the same age that have been interpreted either as cognate cumulates [*Shahbazi et al.*, 2010; *Esna-Ashari et al.*, 2011] or as separate magmas [*Ghalamghash et al.*, 2009a, 2009b].

6.3. Post-Jurassic Plutons

Cretaceous intrusives are relatively limited in area, in contrast to the much broader distribution of Jurassic plutons (Table 2 and Figure 7). Three plutonic centers with Early Cretaceous crystallization ages are known from the Qori metamorphic complex east of Neyriz [*Fazlnia et al.*, 2009], the Suffiabad area east of Sanandaj [*Azizi et al.*, 2011b], and from the Qorveh area, between Sanandaj and Hamadan [*Mahmoudi et al.*, 2011]. In the Makran segment of the SSA SE of the Strait of Hormuz, tectonized Jurassic granitoids as young as 153 Ma are cut by E-W trending diabase dikes and are unconformably overlain by Valanginian (140–133 Ma) alkaline lavas and sediments. They are thus either latest Jurassic or earliest Cretaceous in age [*Hunziker et al.*, 2015].

Late Cretaceous granitoids are only common in the northwestern segment of the SSA. Examples include the Hasan Salary granodiorite, south of Saqqez [*Mahmoudi et al.*, 2011], and the Naqadeh gabbrodiorite, northwest of Mahabad (Figure 7) [*Mazhari et al.*, 2011a, 2011b]. Farther northwest, a group of shallow plutons to

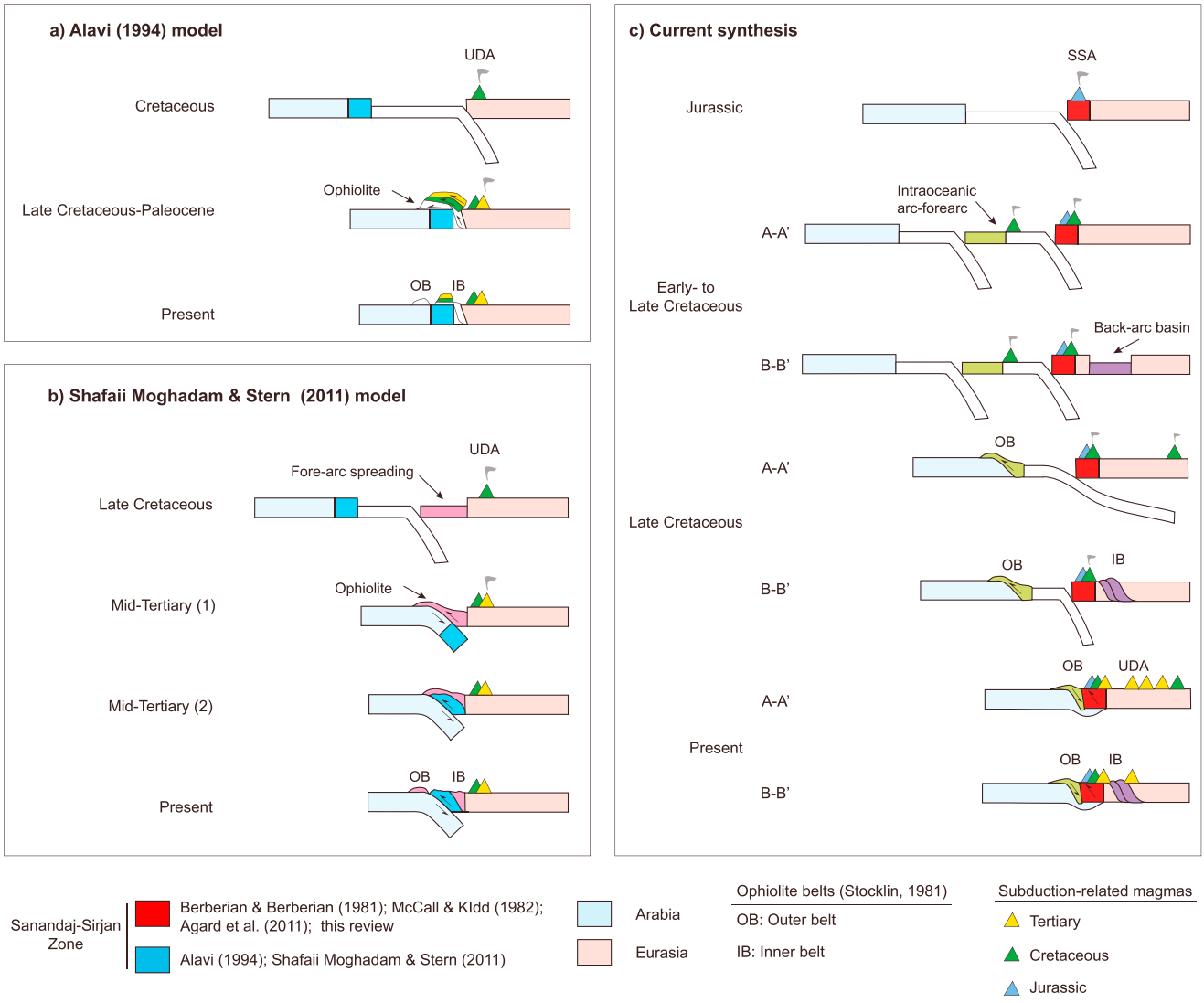

Figure 10. Three hypotheses on the position of the Sanandaj-Sirjan zone relative to the Neotethys Ocean and the origin of its bordering ophiolites: (a) Alavi model, considering the Sanandaj-Sirjan zone on the southern margin of the Neotethys and viewing the igneous-metamorphic rocks of the SSA as nappes transported from the Eurasian side after the collision. (b) Model of *Shafaii Moghadam and Stern* [2011], also positioning the Sanandaj-Sirjan zone on the southern margin of the Neotethys and proposing complete burial of the SSA in the subduction channel before rising underneath a hypothetical fore-arc ophiolitic nappe. (c) The more widely accepted model viewing the Sanandaj-Sirjan zone on the northern margin of the Neotethys based on the Permian-Triassic sedimentary history, development of the Jurassic arc and paleomagnetic data. Positions of sections A-A′ and B-B′ are shown in Figure 1.

the south of Urumieh have yielded K-Ar ages from 110 Ma to 76 Ma [*Ghalamghash et al.*, 2009a, 2009b] (Table 2). In the northernmost SSA near Salmas, mafic to intermediate and felsic plutons intrude Early Cretaceous strata, are overlain by early Tertiary strata, and are presumably Late Cretaceous in age but are as yet undated radiometrically [*Ghaffari et al.*, 2013].

Tertiary magmatism in the SSA is minor, except for Paleocene-Eocene plutonism in the NW segment (Table 2 and Figure 7). Paleocene granodiorites include one body to the south of Saqqez [*Mahmoudi et al.*, 2011] and several large bodies in the Mahabad-Takab region and south of Khoy [*Ghorashi and Arshadi*, 1978; *Kholghi Khasraghi*, 1999; *Eftekharnezhad*, 2004; *Jamshidi Badr et al.*, 2012; *Heidari*, 2014]. Bimodal Paleocene plutonism has been reported to occur to the north of Golpaygan based on K-Ar [*Rachidnejad-Omran et al.*, 2002] and Ar-Ar ages [*Moritz et al.*, 2006]. Plutons of Eocene age include (1) the Gosheh-Tavandasht quartz monzodiorite, located about 350 km SE of Hamadan [*Mahmoudi et al.*, 2011], (2) the Piranshahr massif west of Mahabad [*Mazhari et al.*, 2009], and (3) the Taa-Baysaran [*Azizi et al.*, 2011a] and Marivan [*Sepahi et al.*, 2014] granitoids west of Sanandaj. Several gabbro bodies were emplaced near the Zagros suture in the Late Eocene [*Leterrier*,

1985; *Agard et al*., 2005]. Neogene granitoids are rare in the SSA, and the only well-documented example so far is the Sari Gunay epizonal intrusive system (circa 11–12 Ma), which cuts a latitic to trachytic volcanic complex of the same age, located ~60 km northwest of the city of Hamadan [*Richards et al*., 2006]. From this magmatic center a chain of cinder cones, lava domes, and subvolcanic plugs of Miocene-Quaternary age spreads northwestward for about 200 km (see section 3).

7. Discussion

Reexamination of the current knowledge about the SSA bears on a number of long-debated issues outlined in section 1, perhaps most importantly the question of a north versus south position of the SSA with respect to the Neotethys Ocean in Permian-Triassic time, and the nature and evolution of the arc in post-Triassic time, in particular the subduction kinematics of the Neotethyan oceanic lithosphere. Any paleogeographic model of the SSA hinges critically on interpretations of the origin of its bounding ophiolite bodies, which are primarily younger in age than the main period of arc magmatism, and as such represents a "tectonic overprint" of the arc. Hence, we begin our discussion by outlining the history and origin of these bodies and their implications for the paleogeography of the SSA and then address issues related to the evolution of the arc in Late Paleozoic and Early Mesozoic time.

7.1. Ophiolites

Tethyan ophiolites discontinuously mark the boundaries of the SSA, with the Zagros fold-thrust belt to the SW and the Urumieh-Dokhtar arc in the NE, in the form of outer belt and inner belt ophiolites, respectively (Figure 1) [e.g., *Stöcklin*, 1981]. The outer belt includes coherent, "Oman-like" ophiolites, whereas the inner belt comprises highly fragmented ophiolitic mélanges, also referred to as "colored mélange" [e.g., *Ricou*, 1970; *Stöcklin*, 1974]. The longstanding enigma of the two belts is that on the one hand, igneous components (gabbro plutons, dikes, etc.) in the two belts are restricted to a narrow age span in mid-Cretaceous time (circa 92–102 Ma). On the other hand, although sedimentary components of the inner belt, colored mélange is restricted to mid-Cretaceous age, outer belt sedimentary ages range from Triassic to Cretaceous [e.g., *Davoudzadeh*, 1972; *Ricou*, 1970; *Braud*, 1990].

Despite the marked contrast in sedimentary age range of the inner and outer belts, some workers have correlated the two belts, suggesting that the Zagros ophiolites formed in the inner belt position, northeast of the SSA, and reached their present positions between the SSA and the edge of the Arabian plate by large-scale, SE-directed overthrusting (Figures 10a and 10b). This hypothesis implies that the SSA originally lay adjacent to the Arabian plate along the southern margin of the Neotethys Ocean [e.g., *Pamic et al*., 1979; *Alavi*, 1980, 1994]. Taking the hypothesis a step further, *Shafaii Moghadam and Stern* [2011] suggested that subduction initiation in the Neotethys Ocean occurred within the Urumieh-Dokhtar arc, rather than within the SSA. In their model, the entire SSA was a fragment along the NE margin of Arabia partially subducted toward the NE, underneath a contiguous sheet of inner belt and outer belt ophiolites, and then reexhumed, preserving outer belt ophiolites as klippe along its SW margin.

These hypotheses are perhaps best evaluated by a comparison of sea-floor spreading histories implied by these ophiolites. Ophiolites may represent the crust and upper mantle in either open oceans or small marginal basins, and the first-order guide to distinguishing the two stems from the type of the associated sediments, not their magmatic components [e.g., *Robertson*, 2002]. Marginal basins are generally narrow and short-lived, and their proximity to surrounding high-standing lithosphere inhibits the development of typical abyssal plain deposits such as radiolarian chert and red clays, in favor of spicular chert and turbiditic sedimentation. The Oman ophiolite, which together with the Zagros outer belt ophiolites form "Le croissant ophiolitique peri-Arabe" of *Ricou* [1970] is so radiolarite-rich that it is also referred to as an "ophiolite-radiolarite belt" [*Alleman and Peters*, 1972]. The Pichakun radiolarite series and Bakhtegan beds in the Neyriz ophiolite (Figure 1) is an age equivalent of the Late Triassic-Late Cretaceous Hawasina nappe complex of deep-sea sediments in Oman, which reaches structural thicknesses of over 2 km [*Ricou*, 1970; *Hallam*, 1976; *Robin et al*., 2010]. Analogous to the Pichakun Series, the Kermanshah radiolarites (Figure 1) constitute a structurally thick (>3000 m) nappe complex, repeating the same stratigraphically thin (<300 m) but temporally complete sequence of Triassic-Cretaceous deepwater units [*Braud*, 1978; *Gharib and De Wever*, 2010]. The long (>130 Myr) duration of deepwater sedimentation suggested by the Oman-Zagros radiolarites indicate

prolonged residence in an open-ocean environment, regardless of any differences that may exist in the origin of their igneous components [e.g., *Whitechurch et al*., 2013].

In contrast to the outer belt ophiolites, the volumetrically minor radiolarites in the inner belt ophiolites are restricted in age to the mid-Cretaceous. Dated components of the colored mélange radiolarites include lowermost Coniacian strata in the Khoy area [*Pessagno et al*., 2005], Aptian-Albian in the Gazik area, East Iran [*Babazadeh and De Wever*, 2004], Albian-Cenomanian in the Birjand area, East Iran [*Babazadeh*, 2007], and mid-Albian and Turonian in the Ashin area north of Nain [*Shirdashtzadeh et al*., 2015]. Radiolarian ages are not available for the Nain-Dehshir-Shahrebabak-Baft chain of ophiolites, but they are also probably Cretaceous based on the presence of Late Cretaceous fossils in associated pelagic limestones [e.g., *Davoudzadeh*, 1972; *Stöcklin*, 1981]. Therefore, small volume radiolarites in the inner belt ophiolites and their relatively short depositional time spans support formation of the colored mélange in short-lived, narrow, embryonic marginal basins (Figure 10c). We therefore interpret the inner belt ophiolitic assemblages as distinct from the outer belt or Zagros ophiolites, which clearly formed in an open ocean with a long history of seafloor spreading.

7.2. North Versus South Tethyan Position of the Sanandaj-Sirjan Zone

Although most geologists who have worked in Iran regard the SSA as having developed on the northern margin of the Neotethys Ocean [e.g., *Stöcklin*, 1968, 1974; *Takin*, 1972; *Berberian and King*, 1981; *Berberian and Berberian*, 1981; *Tillman et al*., 1981; *Dercourt et al*., 1986; *Agard et al*., 2005; *Ghasemi and Talbot*, 2006; *Mohajjel and Fergusson*, 2014], as alluded to above there are models which place the zone together with the Zagros domain along the southern margin of the Neotethys Ocean [e.g., *Alavi*, 1994]. Reexamination of these models is informative in that almost all models draw a contrast between the complexity of Mesozoic stratigraphy and structure of the SSA, versus the relative simplicity of the neighboring Zagros fold-thrust belt. Indeed, this contrast inspired early workers to name the SSA "the Complex Belt" [e.g., *Harrison*, 1968]. The relative complexity of the SSA stems partly from the presence of ophiolites along its margins (Figure 1) but also from the presence of unconformities and volcanic rocks in late Paleozoic and Mesozoic successions, and extensive metamorphism and plutonism of diverse age, none of which is observed in the Zagros fold and thrust belt.

In an initial version of a model that excludes Neotethyan subduction underneath the SSA, the SSA is interpreted as "relict Mesozoic oceanic crust overthrust by metamorphic rocks," transported from the northeast [*Adib*, 1978; *Pamic et al*., 1979, Figures 2 and 3]. According to this model, the SSA was attached to the Zagros (i.e., the Arabian subcontinent) throughout the history of the Neotethys Ocean. Subsequently, *Alavi* [1980] reiterated that the MZT cannot represent the Arabia-Eurasia suture and proposed that the calc-alkaline Urumieh-Dokhtar magmatic belt of Late Cretaceous-Tertiary age overlies the ancient southwestern margin of the Eurasian continent, which excludes the SSA. However, he modified the *Pamic et al*. [1979] model by considering the SSA as underlain by a continental crust, rather than oceanic crust. *Alavi and Mahdavi* [1994] revisited the controversy on the location of the Gondwanaland-Asia suture by asserting that similar rock formations occur across the MZT in the Nahavand region (west of Hamadan, Figure 3). However, the fault between these exposures is not the MZT, but rather the Main Recent fault, which cuts across the sinuous trace of the MZT in this area, such that both of these sections are in fact part of the Arabian plate.

Alavi [1994, Figure 2] presented details in regard to his southwestward overthrusting model, suggesting that the "autochthonous" (i.e., Arabian) part of the SSA is restricted to the passive margin sediments of Permain and Triassic age (Figure 10a). He presumed that all metamorphic units and volcanic-bearing post-Triassic strata, including the Hamadan phyllites, are "allochthonous." The stratigraphic and intrusive superposition of the extensive calc-alkaline Jurassic volcanics and intrusives of the SSA with pre-Jurassic rocks, including intrusive relationships of arc batholiths into the pre-Jurassic substrate (e.g., Figure 4), and stratigraphic and structural continuity across the Triassic-Jurassic boundary reported in many previous studies [e.g., *Zahedi*, 1976; *Berberian and Berberian*, 1981; *Kazmin et al*., 1986] are not accounted for in the model. *Alavi* [1994] also suggested that the thick crust and relatively high mean elevation of the SSA were caused by south directed imbrication of up to 15 km of nappes composed of fragments of the Cretaceous and younger arc (Figure 10a), as opposed to underthrusting of the leading edge of the Arabian plate advocated by most workers [e.g., *Bird et al*., 1975; *Giese et al*., 1984; *Paul et al*., 2010; *Allen et al*., 2013].

The alternative to the *Pamic et al*. [1979] and *Alavi* [1994] models put forward by *Shafaii Moghadam and Stern* [2011, Figure 2b], which also equates the Nain-Baft and Neyriz-Kermanshah ophiolites, suggests that both ophiolitic belts initially formed together in a fore-arc setting to the north of the SSA and were later transported tectonically onto the Arabian plate, as mentioned above (Figure 10b). The thrusting in their model must have happened before the Late Cretaceous to allow (1) shedding ophiolitic detritus into the Late Cretaceous-Eocene foreland basins along the high Zagros (in the Amiran, Kashkan, and Sachun Formations) [*Saura et al*., 2011; *Allen and Talebian*, 2011] and (2) unconformable onlap of the ophiolite by Late Cretaceous marine sediments (e.g., Tarbur Formation at Neyriz) [e.g., *Hallam*, 1976]. The model thus requires closing of the Zagros-Central Iran oceanic gap by the Late Cretaceous. According to *Shafaii Moghadam and Stern* [2011], the SSA comprises exhumed, offscraped sediments of the Arabian plate, which now define an anticlinorium structurally beneath the fore-arc ophiolites preserved along its margins.

The interpretation of *Shafaii Moghadam and Stern* [2011] and similar models has little explanatory power in regard to the primary geological features observed in the SSA, including (1) extensive, structurally thick exposures of Pan-African crystalline basement; (2) the latitudinal history of the SSA relative to Arabia and Eurasia defined paleomagnetically; (3) the Permian-Triassic passive margin sediments; (4) the overlying Jurassic volcanics; (5) the chain of calc-alkaline Jurassic granitoids; and (6) the widespread preservation of unmetamophosed and low-*P* metamorphic rocks. This model views the SSA as tectonic sliver along the leading edge of the Arabian plate that was partially subducted and then returned to the surface in a subduction channel, in a mode we would liken to the analog models of *Chemenda et al*. [1996, 2000] to describe the evolution of high-pressure assemblages in the Oman Mountains, Himalaya, and other belts. To the contrary, we stress the lack of any evidence for even low-temperature metamorphism characteristic of subduction channels (lawsonite, carpholite, and glaucophane-bearing assemblages) in stratigraphic successions typical of the SSA (Figures 4 and 5). As noted above, evidence for higher-temperature subduction channel facies (jadeite, ompahcite, etc.) are also wholly lacking, with the lone exception of the Shahrekord area eclogites which are likely Pan-African, and the Hajiabad blueschists and similar rocks. The latter, although Late Cretaceous in age, are thin tectonic slivers associated with outer belt ophiolitic masses along the Main Zagros suture zone, and most likely developed in a subduction channel structurally beneath the SSA, not above it. These metamorphic assemblages do not affect archetypal sediments of the SSA. Moreover, the model claims that initiation of Neotethyan subduction could not have occurred earlier than Late Cretaceous time, in contradiction to the voluminous calc-alkaline arc magmatism of Jurassic age described in section 6.

Yet a different model considers existence of two Neotethys Oceans [*Glennie*, 2000]. According to this model, Neotethys 1 had been created by the rifting of the Cimmerian continental ribbon from Arabia in the Late Permian, and Neotethys 2 had formed in the Late Triassic by separating the Sanandaj-Sirjan zone from Central Iran. The idea of Neotethys 2 obviously infers that the inner-belt Khoy and Nain-Baft ophiolites are remnants of a continuous Neotethys 2 ocean. However, in the 1000 km gap between these two inner-belt ophiolites, there are no suture markers (Figure 1), and a stratigraphic gradation between the SSA and Central Iran is apparent anywhere that the border zone is not covered by the younger sediments. These patterns suggest that the putative "Neotethys 2" was not a through-going ocean analogous to Neotethys 1 but was instead a series of marginal basins (shown schematically in Figure 8e). As noted in the previous section, oceanic sediments older than Late Cretaceous are absent from those ophiolites. Therefore, it is more reasonable to view the Neotethys 2 as discontinuous, short-lived suprasubduction extensional basins along the northeastern margin of the SSA (Figure 8e). *Ghasemi and Talbot* [2006] viewed the gap between the two ophiolites as a temporary northwestward extension (or a failed rift arm) of a Cretaceous Nain-Baft Ocean.

7.3. Polarity of Subduction

North dipping subduction of Neotethyan oceanic lithosphere, as a general explanation of the Jurassic-Tertiary calc-alkaline magmatism along the SSA and Urumieh-Dokhtar zone seems to be robust. However, south dipping subduction of the Paleotethys oceanic lithosphere from the north, in latest Triassic-Early Jurassic time, has also been proposed [*Sengör*, 1979, Figure 2; *Sengör et al*., 1993]. The primary motivation for assuming a south dipping subduction zone is to provide a mechanism for the opening of the Neotethys Ocean as a back-arc basin over an earlier subduction zone. However, this explanation faces timing problems: (1) closure of the Paleotethys was already completed in the Late Triassic [e.g., *Horton et al*., 2008] and (2) opening of the Neotethys was underway in Early Permian time [e.g., *Alirezaei and Hassanzadeh*, 2012],

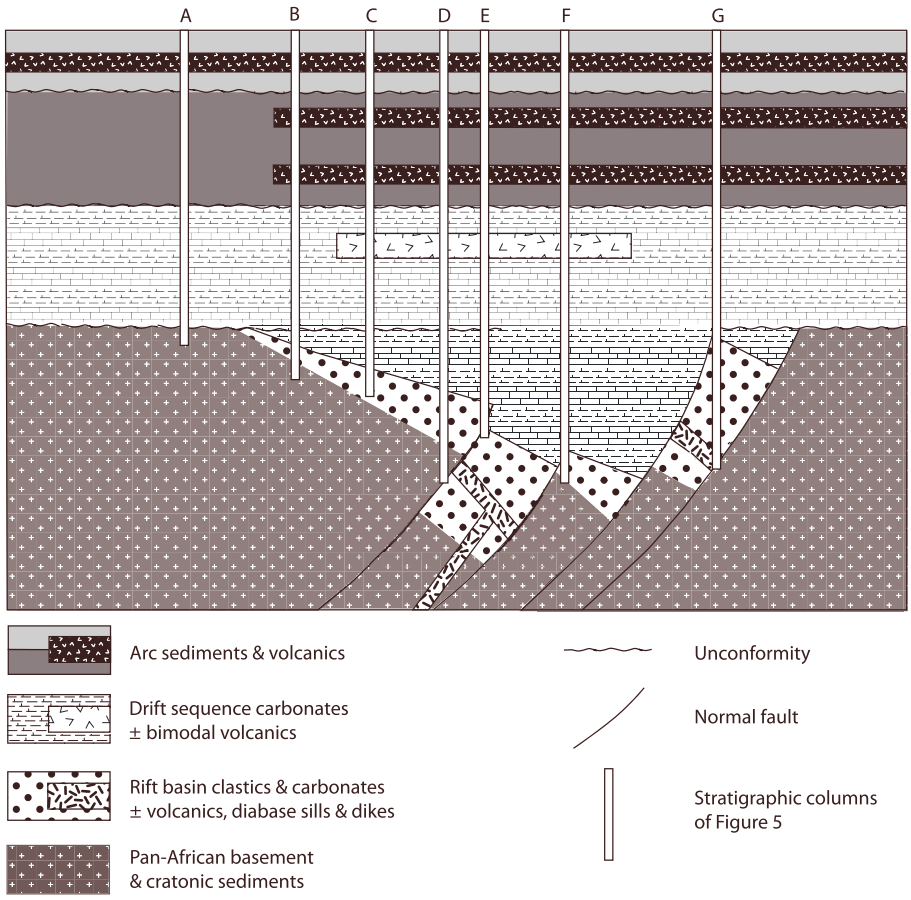

Figure 11. Conceptual model of tectonostratigraphic architecture of the Sanandaj-Sirjan zone, showing a Late Carboniferous (?)-Early Permian continental rift basin sequence followed by (1) thick, concordant deposition of passive margin sediments and (2) unconformably overlying continental arc successions of Jurassic age. Vertical bars show sections from Figure 5 used to construct the diagram.

and therefore, magmatism of Late Triassic or Early Jurassic age within the SSA is too young to be caused by southward subduction of Paleotethyan lithosphere. The other motivation for proposing south dipping subduction is to explain widespread pre-Shemshak tectonic deformation and the folding of Barrovian metamorphic rocks in the southeastern SSA as a consequence of Late Triassic-Early Jurassic collision of the northern margin of the Cimmerian continent with Asia [*Sengör*, 1979; *Sengör et al*., 1993]. Attributing those features to the closing of Paleotethys does not explain why the most intense tectonic deformation and metamorphism are on the southern margin of the Cimmerian continent rather than to the north [*Sengör*, 1979]. Furthermore, the Late-Early to Middle Jurassic age of peak of metamorphism in the southeastern SSA [*Fazlnia et al*., 2007; *Sheikholeslami et al*., 2008; *Alizadeh et al*., 2010], although still not well constrained, postdates closing of the Paleotethys Ocean.

Based on these considerations, we depict closure of the Paleotethys Ocean to have occurred on both south and north dipping zones (possibly, either one or the other could have acted alone), active until Late Triassic time (Figures 8a–8c). As noted above, some models assign the SSA to a different overall paleogeographic realm than terrains farther north (Central Iran, Alborz Mountains, etc.), in part due to the presence of the inner belt ophiolites [e.g., *Sengör et al*., 1993; *Alavi*, 1994; *Shafaii Moghadam and Stern*, 2011]. In contrast, we consider the SSA as the southern margin of a relatively coherent microcontinent, or continental ribbon, that was disrupted by rifting that led to the formation of the inner belt ophiolites, restricted to mid-Cretaceous time.

7.4. Patterns of Subsidence and Uplift Since the Permian

The position of the Earth's surface relative to mean sea level through geologic time is recorded in shallow marine deposits, and by that principle, such sedimentary rocks tell us when a given continental location

was near sea level [*England and Molnar*, 1990]. The Permian and Triassic were a time of major subsidence for the SSA. The observed thickening of the Permian and Triassic sections toward the Zagros suture, and the relatively thick, conformable sedimentation during this time along the "axis" of the basin constitutes compelling evidence that these sequences represent facing passive margins along the flanks of the Neotethys Ocean (Figures 6 and 8). This hypothesis is supported by the fact that lower Permian sections in the SSA are dominated by nonmarine siliciclastic sedimentation accompanied by bimodal volcanics and diabase sills, and the mid-Permian through Triassic sections are predominantly marine, suggesting a transition from active continental rifting to drift subsidence occurred in mid-Permian time (Figures 5, 6, and 11). Local subaerial exposure in the Late Permian, suggested by karstification of the platform carbonates and formation of laterites [*Eftekharnezhad*, 2004], may indicate exposure along a flexurally uplifted rift shoulder. Wholesale emergence, however, took place in the Late Triassic, as evidenced by the regional unconformity at the base of the Shemshak Formation, as well as its predominantly continental depositional environment.

The Jurassic was a time of magmatic arc construction, diversification of sedimentary basins, and formation of deep troughs that accommodated thick sequences ranging from continental deposits to marine, volcanic-rich flysch and carbonates, all unconformably overlain by Barremian-Aptian *Orbitolina*-bearing limestones (Figures 3 and 5). In addition to radiometric ages on igneous bodies, the stratigraphic transition beginning near the base of the Jurassic, when widespread calc-alkaline volcanism and volcaniclastic sedimentation began to predominate in the SSA, is the primary signature of the transition from passive margin sedimentation to the development of a Japan-type or Andean-type magmatic arc (Figures 5, 10, and 11). After the Permian and probable Triassic rift-related crustal thinning, Jurassic calc-alkaline volcanism and the associated magmatic underplating (1) thickened the crust from top and bottom and (2) reestablished normal continental crustal thicknesses, as indicated by the chemistry of the granitoids [e.g., *Fazlnia et al*., 2007; *Esna-Ashari et al*., 2012]. It is not yet clear what the state of stress was within the calc-alkaline arc during most of its development, except as mentioned above there was a profound arc-normal crustal shortening event prior to mid-Cretaceous marine sedimentation. Shallow marine conditions prevailed in the belt through most of the Cretaceous, and the extensive platform carbonates of this period register the last regional submergence of the belt.

The Paleocene was a time of continental erosion, with relatively emergent conditions that led to the widespread deposition of nonmarine conglomeratic deposits. Surface uplift of the SSA continued in the Eocene with limited marine encroachment mostly affecting the borders. Local outcrops of nummulitic limestones within mainly continental sedimentary and volcanic deposits fringing the SSA imply emergence as elongate islands or an archipelago. Such a pattern of partial uplift was sustained until the early Miocene. Deposition of the marine Qom Formation occurred on the still-subsiding northeastern border of the SSA, and in the waning Neotethyan trench to the southwest. Surface uplift which started in Late Cretaceous-early Paleocene time did not result in highly elevated terrain until after deposition of the Qom Formation in post Early Miocene time (~20 Ma), presumably resulting from syncollisional crustal thickening. Buoyancy of the thickened lithosphere in Paleogene time may have been mitigated or counteracted by continental extension, such as that identified in the Golpaygan and Mahallat regions [*Verdel et al*., 2007, 2013], perhaps driven by thermal weakening of the lithosphere in the wake of the Palegene plutonism in the NW part of the SSA (Table 2 and Figure 6).

The sluggish Paleogene uplift was suddenly accelerated at ~20 Ma due to collisional underthrusting of the Arabian continent [e.g., *McQuarrie et al*., 2003; *Paul et al*., 2010; *Mouthereau*, 2011]. This is also the time of the first arrival of SSA-derived detritus on the nearby foreland basins in the High Zagros [e.g., *Fakhari et al*., 2008]. Although the Qom Formation marks a maximum age for the time of wholesale uplift above sea level, two limitations exist: (1) the long time span (~18 Myr) from the Oligocene to Early Miocene for the ages of the unit and (2) the rarity of any Tertiary marine deposits in the axial part of the SSA, possibly indicating that at least parts of it were well above sea level before Qom deposition.

7.5. Hypothesis of a Two-Part Sanandaj-Sirjan Zone and Its Validity

Some geologists have subdivided the SSA into two parts along its strike (northwest and southeast), with a boundary near the latitude of Golpaygan, based on putative differences in their tectonic, metamorphic, and plutonic histories [e.g., *Ghasemi and Talbot*, 2006; *Arfania and Shahriari*, 2009]. The assumption of segmentation of the SSA started with the definition of a "Hamadan-Urumieh subzone" [*Huber and Eftekharnezhad*, 1977], characterized by a narrow, deep trough in the Jurassic and Cretaceous formed in the aftermath of a Late Triassic collision, accommodating thick sequences of volcano-sedimentary flysch-like

volcanosedimentary deposits (Hamadan phyllite and Sanandaj slate), which then underwent extensive granitic intrusion and tectonic deformation in Late Cretaceous to Early Tertiary time [*Eftekharnezhad*, 1981]. As noted earlier the timing of the granitic magmatism and metamorphism is mostly older than originally supposed (Jurassic-Early Cretaceous with only local continuation in the Late Cretaceous-Paleocene; Tables 2 and 3; Figures 7 and 9). We concur that the Hamadan-Urumieh subzone is a rapidly subsiding extensional trough, but in the context of renewed rifting, perhaps driven by the initiation of the postcollision subduction system (Figure 6c) [e.g., *Gurnis et al*., 2004]. In any event, parts of the SSA southeast of Golpaygan are not fundamentally different from the Hamadan-Urumieh segment, because the entire SSA is characterized by rapidly subsiding Jurassic-Cretaceous basins where subduction-related volcanic rocks are extensively interlayered with thick sequences of marine and continental sediments (Figure 5), possibly in an overall rifting environment. Jurassic granitoids are also numerous in the southeastern SSA and, as is the case to the northwest, locally constitute large batholiths. The Jurassic plutons with U-Pb zircon emplacement ages in the proposed southeastern segment include the Kolah Ghazi [*Chiu et al*., 2013], Qori [*Fazlnia et al*., 2009], Chah Dozdan and Chah Bazargan [*Fazlnia et al*., 2007, 2013], Siahkuh [*Arvin et al*., 2007], and Sargaz [*Chiu et al*., 2013] complexes. The Jian granite in the Abadeh region also has a suggested Jurassic age [*Shahidi*, 2000] but has not yet been dated. Although there is no clear distinction between the northwestern and southeastern parts of the SSA with regard to the main Jurassic magmatic episode, the northwesternmost part is distinguishable from the remainder of the SSA because of magmatism in Cretaceous-Paleogene times.

Another basis for subdividing the SSA has been variations in timing of deformation and metamorphism: Late Cretaceous in the northwestern part versus Middle to Late Triassic in the southeastern part [*Ghasemi and Talbot*, 2006]. This suggestion is not supported by (1) the three independent metamorphic episodes that occurred in the southeast (Table 1) [e.g., *Berberian*, 1977], (2) extensive metamorphism of strata of Jurassic age [*Watters et al*., 1970; *Mousivand et al*., 2011], and (3) the abundance of Jurassic batholiths mentioned above. In addition, tectonic deformation and metamorphism have occurred in multiple episodes everywhere in the belt, and both NW and SE segments contain examples of metamorphism in both Jurassic and Late Cretaceous time [*Berberian et al*., 1981; *Berberian and King*, 1981; *Mohajjel and Fergusson*, 2000].

7.6. Neotethyan Arc Magmatism: Spatiotemporal Evolution and Implications for Metamorphism

The SSA is dominated by relatively uniform shallow carbonate shelf/ramp sedimentary environments of Permain and Triassic age with possible local basaltic or bimodal magmatism, suggestive of an Atlantic-type continental margin (Figure 11). Near the Triassic-Jurassic boundary (~200 Ma), the system changed markedly, to a rift (?) basin system containing diverse sedimentary environments dominated by thick, calc-alkaline volcanosedimentary sequences, variably spanning Jurassic and Lower Cretaceous time. At present, most of these sections are well dated paleontologically [e.g., *Aghanabati*, 2014]. U-Pb zircon dates that constrain depositional age of the Jurassic strata, and geochemical data on the volcanics, are few, but in conjunction with paleontological ages, they are nonetheless sufficient to support the general conclusion that the system makes a transition from a mature (circa 80–100 Myr old) passive margin to a nascent magmatic arc near the beginning of Jurassic time (Figures 5 and 11).

Existing radiometric ages for the Jurassic volcano-sedimentary succession are sparse but have been determined for metamorphosed felsic volcaniclastic sediments or lavas between Abadeh and Sirjan (Tables 1 and 3 and Figure 7). These include the detrital zircon age of 191 ± 12 Ma from the Surian metamorphic complex to the east of Abadeh, mentioned above [*Mousivand et al*., 2012], and two ages for magmatic zircons in metarhyodacites from the Chah Gaz metamorphic complex to the NE of Neyriz, with a mean age of 174 ± 1.2 Ma [*Mousivand et al*., 2011]. Because the dated volcanics have evolved compositions, they probably represent a mature stage in the history of the arc. In the well-studied modern arcs, such as the Izu-Bonin-Mariana arc, a time lag of ~10 Myr has been documented to exist between the initial decompression melting of the mantle and to form the first MORB-like (i.e., primitive or boninitic) arc basalts, and normal, andesitic arc magmatism [*Ishizuka et al*., 2011]. Accordingly, we suggest that the voluminous MORB-like arc basalts in Sirjan-Hajiabad-Jiroft area [*Sabzehei et al*., 1994; *Monsef et al*., 2010] could have erupted as early as latest Triassic-Early Jurassic time. We interpret the Sargaz (175 Ma) [*Chiu et al*., 2013] and the Siahkuh granitic batholiths [*Arvin et al*., 2007] in this same area as more evolved products of the mature arc magmatic stage.

Consideration of the remarkably continuous geographic distribution of the arc plutons (Figure 7) bears strongly on previous concepts of the origin of these magmas that require reappraisal. First, after initiation of the arc, the plutonic belt occupied a strike length of at least 1200 km along the arc, from the Qorveh area

(in the northwest) to the Jiroft area (in the southeast) during Early to Late Jurassic time (Figures 7 and 9). Jurassic plutonism also occurs in the southeastern tail of the SSA in the Makran [*Hunziker et al*., 2015]. This observation contrasts with a previous view that the Jurassic plutonic belt (i.e., Alvand-like granitoids) is restricted to the northwestern half of the SSA (Figure 6) [e.g., *Eftekharnezhad*, 1981; *Mohajjel and Fergusson*, 2014].

A second key point in regard to the distribution of plutons is that the transformation from passive margin to arc did not occur simultaneously along the entire length of the SSA. Indeed, for the arc segment northwest of the Qorveh area, the transformation appears not to have been recorded until the Early Cretaceous (Figure 7). The rarity of the Cretaceous plutons along the Qorveh-Jiroft segment of the belt has been interpreted as the result of inland migration of the arc by slab flattening [e.g., *Berberian and Berberian*, 1981; *Verdel et al*., 2011]. We thus interpret the cessation of arc magmatism in the Cretaceous between Qorveh and Jiroft to reflect slab segmentation, where the slab flattens to the SW while maintaining a "normal" dip beneath areas to the NE where magmatism continued well into the Cretaceous [e.g., *Asnaashary et al*., 2009].

A third significant outcome of this reappraisal is to emphasize that previously unknown Paleogene arc activity in the northwestern SSA between Qorveh and Khoy extends to the NW into Iraq (Table 2 and Figures 7 and 9). This raises the question of how Paleogene arc activity in the SSA is to be explained if the Urumieh-Dokhtar (UDA in Figure 10) arc to the north was operating at the same time. Two obvious possibilities include the following: (1) the slab retained its initial steep dip angle in this northwestern segment. This explanation is supported by the conspicuous scarcity of Paleogene arc rocks in the neighboring segment in the Urumieh-Dokhtar zone [e.g., *Stöcklin and Nabavi*, 1973]. Or (2) a change in slab dip along strike, with a flattened segment resulting in weak magmatism in the UDA, and a steep segment under the SSA to explain the local renewal of magmatic activity during this period [*Whitechurch et al*., 2013; *Ali et al*., 2013].

The metamorphic history is still the least investigated aspect of the SSA, and as the data summarized in Table 1 shows that the ages of both protoliths and metamorphic events for most complexes are in dispute. However, the age of plutonic events are well constrained in most cases and can be used for setting reasonable limits on the timing of at least the high-*T*, low-*P* regional metamorphism, as the magmatic intrusions bring heat up to midcrustal and shallower environments. Early to Middle Jurassic plutonism is the obvious primary source of heat for increasing average crustal temperature. The occurrence of the Jurassic batholiths around the metamorphic complexes in the Qorveh-Aligoodarz and the Neyriz-Sirjan-Hajiabad-Jiroft sections is a strong argument in support of Jurassic metamorphism, although applying modern techniques (such as U-Th-Pb dating of monazites in metapelites) is still necessary for each specific metamorphic complex. In the northwest, where Cretaceous and Paleocene plutonism was significant, younger ages for the latest regional metamorphism are perhaps expected. Indeed, Tertiary metamorphism related to coeval batholith emplacement has been documented using U-Th-Pb dating of monazite in garnet metapelites in the Sursat complex [*Jamshidi Badr et al*., 2012].

8. Summary

The SSA marks the southwestern edge of a continental ribbon within the otherwise oceanic Neotethyan subduction system in Iran. It records the Permian breakup of Gondwanaland, the Permian-Triassic drift history of the Cimmerian continent, latest Triassic/Early Jurassic subduction initiation, and the Jurassic through Paleogene propagation of arc magmatism along the southern margin of Eurasia (Figures 10c and 11). The stratigraphic record reviewed in this paper suggests that the pre-Permian substrate in the SSA includes both Pan-African basement and Paleozoic cratonic sedimentary cover, similar to relations in Central Iran and Arabia. Collectively, they support a pre-Permian paleogeography where all of the various tectonostratigraphic terrains in the modern Iranian collage were derived from a physically continguous region along the northern flank of Gondwanaland. Continental rifting was part of the larger-scale Pangea breakup process, which took place in Late Carboniferous-Early Permian times in Iran, based on timing of emplacement of rift-related granites in Khalifan and Hassan Robat, and extensional deformation preserved in the High Zagros south of the MZT suture. Between what is now the High Zagros and the SSA, the Neotethys Ocean opened, resulting in deposition of two continental margin terrace wedges facing each other during Permian-Triassic time, while the SSA drifted relatively northward. In this period, the Zagros was entirely amagmatic. The SSA experienced some magmatic activity during this time, which remains obscure in terms of magma chemistry, and temporal and spatial dimensions.

Metamorphism of the Paleozoic-Mesozoic cover rocks is generally subgreenschist to low greenschist facies but locally increases to Buchan-type amphibolite facies near Jurassic to Paleocene batholiths. Barrovian-type metamorphism is restricted to fault-bounded basement blocks exhumed either by extensional detachment within the SSA or thrust uplift near the MZT. Most of these fault-bound blocks are traditionally assumed to consist of early or middle Paleozoic age rocks based on lithological correlation with known, unmetamorphosed formations elsewhere, or on the basis of K-Ar dating. However, protolith ages in carefully investigated examples thus far have turned out to be Precambrian. High-pressure metamorphism is highly localized and is either of likely Pan-African age or associated with the ophiolitic slivers.

Initiation of subduction along the northern margin of the Neotethys occurred in Early Jurassic—or perhaps latest Triassic—based on the age of deposition of thick volcanosedimentary strata and emplacement of calc-alkaline magmas in the SSA, following the closure of the Paleotethys Ocean in northern Iran by the Late Triassic. Arc volcanics in the SSA have received less attention for geochemical and geochronological research than the plutons, mostly due to their alteration or metamorphism. However, there is a growing database on the timing of arc plutonism, and existing U-Pb zircon ages show a strong frequency peak near 170 Ma (Middle Jurassic). Arc magmatism continued in the Cretaceous and generated volcanics, mostly near the NW and SE extremes of the SSA, which by then had transformed into a full-fledged ~2000 km long arc. Cretaceous plutons are, however, more concentrated in the northwestern part where Paleocene-Eocene magmatism is also common. If arc magmatism in the Urumieh-Dokhtar zone was the result of inland migration of the arc by slab flattening in the Cretaceous, then the Paleogene arc activity in the northwestern SSA and NE Iraq may have required the formation of a second subduction zone SW of the flat slab segment.

Ophiolites discontinuously mark the SSA borders, forming "outer" and "inner" belts, on the basis of their position (SW versus NE) and the nature of their original oceans (long-lived versus short-lived). Even through igneous components in both belts are predominantly Late Cretaceous (99 to 93 Ma), the oceanic sediments in the outer belt (Zagros) ophiolites record a Triassic to Cretaceous history similar to that of the Oman ophiolite, suggesting formation in a long-lived ocean basin. In contrast, sediments associated with the inner belt (Khoy and Dehshir-Baft) ophiolites indicate sedimentary environments in small ocean basins created by short-lived fragmentation of the Cimmerian continental ribbon.

Based on the data and interpretations presented above, it appears that the SSA does indeed document the fact that an ancient passive margin, albeit on a relatively narrow (approximately 500–1000 km) continental ribbon, may indeed transform directly into an Andean- or Japan-type magmatic arc, a process generally deemed unlikely to occur on the basis of physical modeling [*Gurnis et al*., 2004]. Despite this physical improbability, "direct" conversion is the only simple way that these margins can form. Such conversions appear to have occurred not only in the Mesozoic Neotethys Ocean as proposed here but also along various circum-Pacific continental margins over the last 500 Ma. Indeed, based on our own review of the geologic record of the SSA, the early Mesozoic transition from passive margin to arc along the northern margin of the central Neotethys Ocean may well merit priority for more detailed study. It appears to be an archetypal natural example of a pivotal stage in the Wilson Cycle that is elsewhere poorly preserved.

Acknowledgments

Writing this review paper would not have been possible before the current surge of geochronological data production which started about 10 years ago, referred to in the reference list along with the maps and reports for the region produced by the Geological Survey of Iran. The quality of the presentation was greatly improved by editorial guidance and constructive reviews from Associate Editor A. Khudoley, G. Topuz, and an anonymous reviewer. Mortaza Pirouz is thanked for helping with the ArcGIS compilations of Figures 3 and 7. This work was partially supported by the Caltech Tectonics Observatory under the auspices of Gordon and Betty Moore Foundation and by NSF grant EAR-14-51055 awarded to B. Wernicke.

References

Adib, D. (1978), Metamorphic complex situated along the southwestern margin of the central- and eastern-Iran microplate, *Neues Jahrb. Palaontol. Abh.*, *156*, 393–409.

Agard, P., J. Omrani, L. Jolivet, and F. Mouthereau (2005), Convergence history across Zagros (Iran): Constraints from collisional and earlier deformation, *Int. J. Earth Sci.*, *94*, 401–419.

Agard, P., P. Monie, W. Gerber, J. Omrani, M. Molinaro, B. Meyer, L. Labrousse, B. Vrielynck, L. Jolivet, and P. Yamato (2006), Transient, synobduction exhumation of Zagros blueschists inferred from P–T, deformation, time and kinematic constraints: Implications for Neotethyan wedge dynamics, *J. Geophys. Res.*, *111*, B11401, doi:10.1029/2005JB004103.

Agard, P., J. Omrani, L. Jolivet, H. Whitechurch, B. Vrielynck, W. Spakman, P. Monie, B. Meyer, and R. Wortel (2011), Zagros orogeny: A subduction-dominated process, *Geol. Mag.*, *148*, 692–725.

Aghanabati, A. (2014), *Stratigraphic Lexicon of Iran* [in Persian], vol. 4, p. 544, Jurassic, Geological Survey of Iran, Rahi Publishing Office, Tehran.

Ahadnejad, V., M. V. Valizadeh, R. Deevsalar, and M. Rezaei-Kahkhaei (2011), Age and geotectonic position of the Malayer granitoids: Implication for plutonism in the Sanandaj-Sirjan Zone, W. Iran, *Neues Jahrb. Geol. Paläontol. Abh.*, doi:10.1127/0077-7749/2011/0149.

Ahmadi-Khalaji, A. A., D. Esmaeily, M. V. Valizadeh, and H. Rahimpour-Bonab (2007), Petrology and geochemistry of the granitoid complex of Boroujerd, Sanandaj- Sirjan Zone, Western Iran, *J. Asian Earth Sci.*, *29*, 859–877.

Alavi, M. (1980), Tectonostratigraphic evolution of the Zagrosides of Iran, *Geology*, *8*, 144–149.

Alavi, M. (1994), Tectonics of the Zagros orogenic belt of Iran: New data and interpretations, *Tectonophysics*, *229*, 211–238.

Alavi, M., and M. A. Mahdavi (1994), Stratigraphy and structure of the Nahavand region in western Iran, and their implications for the Zagros tectonics, *Geol. Mag.*, *131*, 43–47.
Alavi Naini, M., J. Hajian, M. Amidi, and H. Bolourchi (1982), Explanatory text of the Takab quadrangle map, 1:250,000, *Geological Survey of Iran*, F8, 99 pp.
Ali, S. A., S. Buckman, K. J. Aswad, B. G. Jones, S. A. Ismail, and A. P. Nutman (2013), The tectonic evolution of a Neo-Tethyan (Eocene–Oligocene) island-arc (Walash and Naopurdan groups) in the Kurdistan region of the Northeast Iraqi Zagros Suture Zone, *Island Arc*, *22*, 104–125.
Alirezaei, S., and J. Hassanzadeh (2012), Geochemistry and zircon geochronology of the Permian A-type Hasanrobat granite, Sanandaj-Sirjan belt: A new record of the Gondwana break-up in Iran, *Lithos*, *151*, 122–134.
Alizadeh, A., M. L. Martinez, and K. Sarkarinejad (2010), ^{40}Ar-^{39}Ar geochronology in a gneiss dome within the Zagros Orogenic Belt, *C. R. Geosci.*, *342*, 837–846.
Alleman, F., and T. Peters (1972), The ophiolite-radiolarite belt of the North Oman Mountains, *Eclogae Geol. Helv.*, *65*, 657–697.
Allen, M. B., and M. Talebian (2011), Structural variation along the Zagros and the nature of the Dezful embayment, *Geol. Mag.*, *148*(5–6), 911–924, doi:10.1017/s0016756811000318.
Allen, M. B., C. Saville, E. J.-P. Blanc, M. Talebian, and E. Nissen (2013), Orogenic plateau growth: Expansion of the Turkish-Iranian Plateau across the Zagros fold-and-thrust belt, *Tectonics*, *32*, 171–190, doi:10.1002/tect.20025.
Alric, G., and D. Virlogeux (1977), *Pétrographie et géochimie des roches métamorphiques et magmatiques de la région de Deh Bid–Bavanat, Chaîne de Sanandaj–Sirjan, Iran* [Thèse 3ème cycle]: Grenoble, p. 316, Université scientifique et médicale de Grenoble, France.
Arfania, R., and S. Shahriari (2009), Role of southeastern Sanandaj–Sirjan Zone in the tectonic evolution of Zagros Orogenic Belt, Iran, *Island Arc*, *18*, 555–576.
Arvin, M., Y. Pan, S. Dargahi, A. Malekizadeh, and A. Babaei (2007), Petrochemistry of the Siah-Kuh granitoid stock southwest of Kerman, Iran: Implications for initiation of Neotethys subduction, *J. Asian Earth Sci.*, *30*, 474–489.
Asnaashary, A., J. Hassanzadeh, B. Wernicke, A. K. Schmitt, G. Axen, and B. Horton (2009), Middle Jurassic flare-up and Cretaceous magmatic lull in the central Sanandaj-Sirjan arc, Iran: An analogy with the southwestern United States, *Geol. Soc. Am. Abstr. Progr.*, *41*(7), 481.
Azizi, H., and A. Jahangiri (2008), Cretaceous subduction-related volcanism in the northern Sanandaj–Sirjan Zone, Iran, *J. Geodyn.*, *45*, 178–190.
Azizi, H., and Y. Asahara (2013), Juvenile granite in the Sanandaj–Sirjan Zone, NW Iran: Late Jurassic–Early Cretaceous arc–continent collision, *Int. Geol. Rev.*, *55*, 1523–1540, doi:10.1080/00206814.2013.782959.
Azizi, H., T. Tanaka, Y. Asahara, S. L. Chung, and M. H. Zarrinkoub (2011a), Discrimination of the age and tectonic setting for magmatic rocks along the Zagros thrust zone, northwest Iran, using the zircon U–Pb age and Sr–Nd isotopes, *J. Geodyn.*, *52*, 304–320.
Azizi, H., Y. Asahara, B. Mehrabi, and S. L. Chung (2011b), Geochronological and geochemical constraints on the petrogenesis of high-K granite from the Suffi abad area, Sanandaj–Sirjan zone, NW Iran, *Chem. Erde*, *71*, 363–376.
Azizi, H., S. L. Chung, T. Tanaka, and Y. Asahara (2011c), Isotopic dating of the Khoy metamorphic complex (KMC), northwestern Iran: A significant revision of the formation age and magma source, *Precambrian Res.*, *185*(3–4), 87–94.
Babazadeh, S. A. (2007), Cretaceous Radiolarians from Birjand ophiolitic range in Sahlabad province, eastern Iran, *Rev. Paléobiol. Genève*, *26*, 89–98.
Babazadeh, S. A., and P. De Wever (2004), Radiolarian Cretaceous age of Soulabest radiolarites in ophiolite suite of eastern Iran, *Bull. Soc. Geol. Fr.*, *175*, 121–129.
Baharifar, A. A., H. Moinevaziri, H. Bellon, and A. Pique (2004), The crystalline complexes of Hamadan (Sanandaj–Sirjan Zone, Western Iran): Metasedimentary Mesozoic sequences affected by Late Cretaceous tectono-metamorphic and plutonic event, *C. R. Geosci.*, *336*, 1443–1452.
Bea, F., A. Mazhari, P. Montero, S. Amini, and J. Ghalamghash (2011), Zircon dating, Sr and Nd isotopes, and element geochemistry of the Khalifan pluton, NW Iran: Evidence for Variscan magmatism in a supposedly Cimmerian superterrane, *J. Asian Earth Sci.*, *40*, 172–179.
Berberian, F., and M. Berberian (1981), Tectono-plutonic episodes in Iran, in *Zagros, Hindukush, Himalaya Geodynamic Evolution*, edited by H. K. Gupta and F. M. Delany, pp. 5–32, AGU, Washington, D. C.
Berberian, M. (1977), Three phases of metamorphism in Hajiabad quadrangle (southeastern extremity of the Sanandaj-Sirjan structural zone): A paleotectonic discussion, in *Contribution to the Seismotectonics of Iran (Part III)*, edited by M. Berberian, *Geological Survey of Iran*, 40, pp. 239–260.
Berberian, M., and G. C. P. King (1981), Towards a paleogeography and tectonic evolution of Iran, *Can. J. Earth Sci.*, *18*, 210–265.
Berberian, M., M. Soheili, and M. H. Kholghi (1981), Polymetamorphism at the Aligudarz sheet area (Golpaygan region) and the problem of the Hercynian orogeny along the active continental margin of Central Iran [in Persian], Geol. Surv. Iran, Internal Report, 19 p.
Besse, J., F. Torcq, Y. Gallet, L. E. Ricou, L. Krystyn, and A. Saidi (1998), Late Permian to Late Triassic palaeomagnetic data from Iran: Constraints on the migration of the Iranian block through the Tethyan Ocean and initial destruction of Pangaea, *Geophys. J. Int.*, *135*(1), 77–92.
Bird, P., M. N. Toksoz, and N. H. Sleep (1975), Thermal and mechanical models of continent-continent convergence zones, *J. Geophys. Res.*, *80*, 4405–4416, doi:10.1029/JB080i032p04405.
Boccaletti, M., F. Innocenti, P. Manetti, R. Mazzuoli, A. Motamed, G. Pasquare, F. Radicatidi Brozolo, and E. Amin Sobhani (1976), Neogene and Quaternary volcanism of the Bijar area (western Iran), *Bull. Volcanol.*, *40*, 122–132.
Braud, J. (1978), Geological map of Kermanshah, 1:250,000 scale, Geological Survey of Iran.
Braud, J. (1990), Explanatory text of the Kermanshah quadrangle map, 1:250,000, Geological Survey of Iran, C6.
Chemenda, A. I., M. Mattauer, and A. N. Bokun (1996), Continental subduction and a mechanism for exhumation of high-pressure metamorphic rocks: New modeling and field data from Oman, *Earth Planet. Sci. Lett.*, *143*, 173–182.
Chemenda, A. I., J. P. Burg, and M. Mattauer (2000), Evolutionary model of the Himalaya-Tibet system: Geopoem based on new modelling, geological and geophysical data, *Earth Planet. Sci. Lett.*, *174*, 397–409.
Chiu, H. Y., S. L. Sun-Lin Chung, M. H. Zarrinkoub, S. S. Mohammadi, M. M. Khatib, and Y. Iizuka (2013), Zircon U–Pb age constraints from Iran on the magmatic evolution related to Neotethyan subduction and Zagros orogeny, *Lithos*, *162-163*, 70–87.
Davoudian, A. R., J. Genser, E. Dachs, and N. Shabanian (2007), Petrology of eclogites from north of Shahrekord, Sanandaj-Sirjan Zone, Iran, *Mineral. Petrol.*, *92*, 393–413, doi:10.1007/s00710-007-0204-6.
Davoudzadeh, M. (1972), Geology and petrography of the area north of Nain, Central Iran, Geological Survey of Iran, report No.14.
Dehghani, G., and J. Makris (1984), The gravity field and crustal structure of Iran, *Neues Jahrb. Geol. Palaontol. Abh.*, *168*, 215–229.
Dercourt, J., et al. (1986), Geological evolution of the Tethys belt from the Atlantic to the Pamirs since the Lias, *Tectonophysics*, *123*, 241–315.
Dimitrijevic, M. D. (1973), Geology of Kerman region, Geological Survey of Iran, Yu/52, 334 p.
Edgell, H. S. (1977), The Permian System as an oil and gas reservoir in Iran, Iraq and Arabia, Proceedings of Second Iranian Geological Symposium, Teheran, 161-201.
Eftekharnezhad, J. (1973), Geological map of the Mahabad quadrangle B-4, scale 1: 250,000, Geological Survey of Iran.
Eftekharnezhad, J. (1981), Tectonic division of Iran with respect to sedimentary basins [in Persian], *J. Iran. Petrol. Soc.*, *82*, 19–28.

Eftekharnezhad, J. (2004), Explanatory text of geological map of the Mahabad quadrangle B-4, scale 1: 250,000, Geological Survey of Iran.
England, P., and P. Molnar (1990), Surface uplift, uplift of rocks, and exhumation of rocks, *Geology*, *18*, 1173–1177.
Eshraghi, A. A. (1996), Geological map of Iran sheet 5559-Songhor, scale 1:100,000, Geological Survey of Iran, Tehran.
Esna-Ashari, A., J. Hassanzadeh, and M. V. Valizadeh (2011), Geochemistry of microgranular enclaves in Aligoodarz Jurassic arc pluton, western Iran: Implications for enclave generation by rapid crystallization of cogenetic granitoids magma, *Mineral. Petrol.*, *101*, 195–216.
Esna-Ashari, A., M. Tiepolo, M. V. Valizadeh, J. Hassanzadeh, and A. A. Sepahi (2012), Geochemistry and zircon U–Pb geochronology of Aligoodarz granitoid complex, Sanandaj-Sirjan Zone, Iran, *J. Asian Earth Sci.*, *43*, 11–22.
Etemad-Saeed, N., M. Hosseini-Barzi, M. H. Adabi, N. R. Miller, A. Sadeghi, A. Houshmandzadeh, and D. F. Stockli (2015), Evidence for ca. 560 Ma Ediacaran glaciation in the Kahar Formation, central Alborz Mountains, northern Iran, *Gondwana Res.*, doi:10.1016/j.gr.2015.01.005.
Fakhari, M. D., G. J. Axen, B. K. Horton, J. Hassanzadeh, and A. Amini (2008), Revised age of proximal deposits in the Zagros foreland basin and implications for Cenozoic evolution of the High Zagros, *Tectonophysics*, *451*, 170–185.
Fazlnia, A. N., A. Moradian, K. Rezaei, M. Moazzen, and S. Alipour (2007), Synchronous activity of anorthositic and S-type granitic magmas in the Chah-Dozdan batholith, Neyriz, Iran: Evidence of zircon SHRIMP and monazite CHIME dating, *J. Sci. Islamic Republ. Iran*, *18*, 221–237.
Fazlnia, A., V. Schenk, F. Van Der Straaten, and M. Mirmohammadi (2009), Petrology, geochemistry and geochronology of trondhjemites from the Qori complex, Neyriz, Iran, *Lithos*, *112*, 413–433.
Fazlnia, A., V. Schenk, P. Appel, and A. Alizade (2013), Petrology, geochemistry, and geochronology of the Chah-Bazargan gabbroic intrusions in the south Sanandaj–Sirjan zone, Neyriz, Iran, *Int. J. Earth Sci.*, *102*, 1403–1426, doi:10.1007/s00531-013-0884-6.
Fonoudi, M., and A. Sadeghi (2003), Geological map of Iran sheet 5161-Baneh, scale 1:100,000, Geological Survey of Iran, Tehran.
Gallet, Y., L. Krystyn, J. Besse, A. Saidi, and L. E. Ricou (2000), New constraints on the Upper Permian and Lower Triassic geomagnetic polarity timescale from the Abadeh section (central Iran), *J. Geophys. Res.*, *105*, 2805–2815, doi:10.1029/1999JB900218.
Gansser, A. (1955), New aspects of the geology in Central Iran, in *Proceedings of the 4th World Petroleum Congress, Rome*, Section I/A/5, pp. 280–300.
Ghaffari, M., N. Rashidnejad-Omran, R. Dabiri, B. Chen, and J. F. Santos (2013), Mafic–intermediate plutonic rocks of the Salmas area, northwestern Iran: Their source and petrogenesis significance, *Int. Geol. Rev.*, doi:10.1080/00206814.2013.817067.
Ghalamghash, J., A. Nedelec, H. Bellon, M. Vousoughi Abedini, and J. L. Bouchez (2009a), The Urumieh plutonic complex (NW Iran): A record of the geodynamic evolution of the Sanandaj–Sirjan zone during Cretaceous times—Part I: Petrogenesis and K/Ar dating, *J. Asian Earth Sci.*, *35*, 401–415.
Ghalamghash, J., H. Mirnejad, and H. Rashid (2009b), Mixing and mingling of mafic and felsic magmas along the Neo-Tethys continental margin, Sanandaj-Sirjan zone, NW Iran: A case study from the Alvand pluton, *N. Jb. Miner. Abh.*, *186*, 79–93.
Gharib, F., and P. De Wever (2010), Mesozoic radiolarians from the Kermanshah formation (Iran), *C. R. Palevol.*, *9*, 209–219.
Ghasemi, A., and C. J. Talbot (2006), A new tectonic scenario for the Sanandaj–Sirjan Zone (Iran), *J. Asian Earth Sci.*, *26*, 683–693.
Ghasemi, A., A. Hajhosseini, and M. Hosseini (2006), Geological map of Iran sheet 6155-Chadegan, scale 1:100,000, Geological Survey of Iran, Tehran.
Ghasemi, H., T. Juteau, H. Bellon, M. Sabzehi, H. Whitechurch, and L. E. Ricou (2002), The mafic-ultramafic complex of Sikhoran (central Iran): A polygenetic ophiolite complex, *C. R. Geosci.*, *334*, 431–438.
Ghorashi, M., and S. Arshadi (1978), Khoy quadrangle map, 1:250,000, Geological Survey of Iran, A2.
Giese, P., J. Makris, B. Akasheh, P. Rower, H. Letz, and M. Mostaanpour (1984), The crustal structure in southern Iran derived from seismic explosion data, *Neues Jahrb. Geol. Palaontol. Abh.*, *168*, 230–243.
Glennie, K. W. (2000), Cretaceous tectonic evolution of Arabia's eastern plate margin: A tale of two oceans. In: A.S. Alsharhan and R.W. Scott. (Eds) Middle East Models of Jurassic/Cretaceous Carbonate System, *Soc. Sediment. Geol. (SEPM) Spec. Publ.*, *69*, 9–20.
Grabeljsek, V., S. Cvetic, and M. N. Dimitrijevic (1972), Geological map of Iran sheet 7547-Sabzevaran, scale 1:100,000, Geological Survey of Iran, Tehran.
Gurnis, M., C. Hall, and L. Lavier (2004), Evolving force balance during incipient subduction, *Geochem. Geophys. Geosyst.*, *5*, doi:10.1029/2003GC000681.
Haghipour, A., and A. Aghanabati (1988), Explanatory text of the Serow quadrangle map, 1:250000, Geological Survey of Iran, A3, 56 pp.
Haghipour, A., and A. Aghanabati (1989), Geological map of Iran, scale 1:2,500,000, Geological Survey of Iran, Tehran.
Hallam, A. (1976), Geology and plate tectonics interpretation of the sediments of the Mesozoic radiolarite–ophiolite complex in the Neyriz region, southern Iran, *Geol. Soc. Am. Bull.*, *87*, 47–52.
Harrison, J. V. (1968), Geology [of Iran], in *The Cambridge History of Iran*, edited by W. B. Fisher, pp. 11–185, Cambridge Univ. Press, Cambridge.
Hassanzadeh, J., D. F. Stockli, B. K. Horton, G. J. Axen, L. D. Stockli, M. Grove, A. K. Schmitt, and J. D. Walker (2008), U-Pb zircon geochronology of late Neoproterozoic–Early Cambrian granitoids in Iran: Implications for paleogeography, magmatism, and exhumation history of Iranian basement, *Tectonophysics*, *451*, 71–96.
Hatzfeld, D., and P. Molnar (2010), Comparisons of the kinematics and deep structures of the Zagros and Himalaya and of the Iranian and Tibetan Plateaus and geodynamic implications, *Rev. Geophys.*, *48*, RG2005, doi:10.1029/2009RG000304.
Haynes, J., and H. Reynolds (1980), Early development of Tethys and Jurassic ophiolite displacement, *Nature*, *283*, 561–563.
Heidari, S. M. (2014), Geology, geochronology and source of Touzlar, Arabshah and Ghozalbolagh gold occurrences in Qorveh-Takab region, Unpublished dissertation, Tarbiat Modares University, Tehran, Iran, 484 pp.
Heidari, S. M., F. Daliran, J. L. Paquette, and D. Gasquet (2015), Geology, timing, and genesis of the high sulfidation Au (–Cu) deposit of Touzlar, NW Iran, *Ore Geol. Rev.*, *65*, 460–486, doi:10.1016/j.oregeorev.2014.05.013.
Heydari, E., J. Hassanzadeh, W. J. Wade, and A. M. Ghazi (2003), Permian-Triassic boundary interval in the Abadeh section of Iran with implications for mass extinction: Part 1. Sedimentology, *Palaeogeogr. Palaeoclimatol. Palaeoecol.*, *193*, 405–423.
Horton, B. K., J. Hassanzadeh, D. F. Stockli, G. J. Axen, R. J. Gillis, B. Guest, A. Amini, M. D. Fakhari, S. M. Zamanzadeh, and M. Grove (2008), Detrital zircon provenance of Neoproterozoic to Cenozoic deposits in Iran: Implications for chronostratigraphy and collisional tectonics, *Tectonophysics*, *451*, 97–122.
Hosseini, B., M. Ghorbani, S. M. Pourmoafi, and A. R. Ahmadi (2012), Identification of two different phases of metamorphosed granitoid in Kuh-Sefid Tootak anticline based on U-Pb Age dating, *Geosci. Quarterly J.*, *21*, 57–66, Geological Survey of Iran, Tehran.
Houshmandzadeh, A., and M. Soheili (1990), Explanatory text of the Eqlid quadrangle map, 1:250,000, Geological Survey of Iran, G10, 158 p.
Huber, H., compiler (1977), *Geological Maps of Iran: Scale 1: 1000,000*, National Iranian Oil Company (NIOC), Tehran.
Huber, H., and J. Eftekharnezhad, compilers (1977), *Geological Map of Northwest Iran: Scale 1: 1000,000*, National Iranian Oil Company (NIOC), Tehran.
Hunziker, D., J. P. Burg, P. Pierre Bouilhol, and A. von Quadt (2015), Jurassic rifting at the Eurasian Tethys margin: Geochemical and geochronological constraints from granitoids of North Makran, southeastern Iran, *Tectonics*, *34*, 571–593, doi:10.1002/2014TC003768.

Ishizuka, O., K. Tani, M. K. Reagan, K. Kanayama, S. Umino, Y. Harigane, I. Sakamoto, Y. Miyajima, M. Yuasa, and D. J. Dunkley (2011), The timescales of subduction initiation and subsequent evolution of an oceanic island arc, *Earth Planet. Sci. Lett.*, *306*, 229–240, doi:10.1016/j.epsl.2011.04.006.

Jafarian, M. B., and M. Zamani Pedram (1999), Geological map of Iran sheet 5758-Malayer, scale 1:100,000, Geological Survey of Iran, Tehran.

Jamshidi Badr, M., F. Masoudi, A. S. Collins, and G. Cox (2010), Dating of Precambrian metasedimentary rocks and timing of their metamorphism in the Soursat metamorphic complex (NW IRAN): Using LA–ICP-MS, U–Pb Dating of Zircon and Monazite, *J. Sci.*, *21*, 311–319.

Jamshidi Badr, M., A. S. Collins, F. Masoudi, G. Cox, and M. Mohajjel (2012), The U-Pb age, geochemistry and tectonic significance of granitoids in the Soursat complex, Northwest Iran, *Turk. J. Earth Sci.*, *21*, 1–35.

Jassim, S. Z., and J. C. Goff (Eds.) (2006), *Geology of Iraq*, pp. 485, Dolin, Prague and Moravian Museum, Brno, Czech.

Kazmin, V. G., I. M. Sbortshikov, L. E. Ricou, L. P. Zonenshain, J. Boulin, and A. L. Knipper (1986), Volcanic belts as markers of the Mesozoic-Cenozoic active margin of Eurasia, *Tectonophysics*, *123*, 123–152.

Khalatbari-Jafari, M., T. Juteau, H. Bellon, H. Whitechurch, J. Cotten, and H. Emami (2004), New geological, geochronological and geochemical investigations on the Khoy ophiolites and related formations, NW Iran, *J. Asian Earth Sci.*, *23*, 507–535.

Khodabandeh, A. A., and A. Amini-Fazl (1993), Geological map of Iran sheet 5066-Tasuj, scale 1:100,000, Geological Survey of Iran, Tehran.

Kholghi Khasraghi, M. H. (1999), Geological map of Iran sheet 5362-Irankhah, scale 1:100,000, Geological Survey of Iran, Tehran.

Leterrier, J. (1985), Mineralogical, geochemical and isotopic evolution of two Miocene mafic intrusions from the Zagros (Iran), *Lithos*, *18*, 311–329.

Mahmoudi, S., F. Corfu, F. Masoudi, B. Mehrabi, and M. Mohajjel (2011), U–Pb dating and emplacement history of granitoid plutons in the northern Sanandaj–Sirjan Zone, Iran, *J. Asian Earth Sci.*, *41*, 238–249.

Masoudi, F., B. W. D. Yardeley, and R. A. Cliff (2002), Rb–Sr geochronology of pegmatites, plutonic rocks and a hornfels in the region South-West of Arak, Iran, *J. Sci. Islam Repub. Iran*, *13*, 249–254.

Mazhari, S. A., F. Bea, S. Amini, J. Ghalamghash, J. F. Molina, P. Montero, J. H. Scarrow, and I. S. Williams (2009), The Eocene bimodal Piranshahr massif of the Sanandaj–Sirjan Zone, NW Iran: A marker of the end of the collision in the Zagros orogeny, *J. Geol. Soc. Lond.*, *166*, 53–69.

Mazhari, S. A., S. Amini, J. Ghalamghash, and F. Bea (2011a), The origin of mafic rocks in the Naqadeh intrusive complex, Sanandaj-Sirjan Zone, NW Iran, *Arab. J. Geosci.*, *4*, 1207–1214, doi:10.1007/s12517-010-0142-1.

Mazhari, S. A., S. Amini, J. Ghalamghash, and F. Bea (2011b), Petrogenesis of granitic unit of Naqadeh complex, Sanandaj–Sirjan Zone, NW Iran, *Arab. J. Geosci.*, *4*, 59–67, doi:10.1007/s12517-009-0077-6.

McCall, G. J. H. (1985), East Iran Project, Area no. 1, *North Makran and South Baluchestan*, GSI Rep. No. 57.

McCall, G. J. H. (2002), A summary of the geology of the Iranian Makran, *Geol. Soc. Sp. Pub.*, *195*, 147–204.

McCall, G. J. H., and R. G. W. Kidd (1982), The Makran, southeastern Iran: The anatomy of a convergent plate margin active from Cretaceous to present, in *Trench-Fore Arc Geology*, vol. 10, edited by L. Leggett, *Geol. Soc. London, Spec. Publ.*, *10*, pp. 387–397.

McQuarrie, N., J. M. Stock, C. Verdel, and B. P. Wernicke (2003), Cenozoic evolution of Neotethys and implications for the causes of plate motions, *Geophys. Res. Lett.*, *30*(20), 2036, doi:10.1029/2003GL017992.

Mijalkovic, N., S. Cvetic, and M. N. Dimitrijevic (1972), Geological map of Iran sheet 7148-Sirjan 1:100,000, Geological Survey of Iran, Tehran.

Miyashiro, A. (1973), *Metamorphism and Metamorphic Belts*, George Allen and Unwin, London, 492 pp., ISBN: 978-0-04-550026-0.

Mohajjel, M. (1992), Geological map of Iran sheet 5056-Golpaygan, scale 1:100,000, Geological Survey of Iran, Tehran.

Mohajjel, M., and C. L. Fergusson (2000), Dextral transpression in Late Cretaceous continental collision, Sanandaj–Sirjan Zone, western Iran, *J. Struct. Geol.*, *22*, 1125–1139.

Mohajjel, M., and C. L. Fergusson (2014), Jurassic to Cenozoic tectonics of the Zagros Orogen in northwestern Iran, *Int. Geol. Rev.*, *56*, 263–287, doi:10.1080/00206814.2013.853919.

Monsef, I., M. Rahgoshay, and H. Whitechurch (2011), Petrogenetic variations of the Jurassic magmatic sequences of Hoseinabad-Hajiabad regions in Sanandaj-Sirjan Zone (south of Iran) [in Persian with English abstract], *Petrology*, *1*(4), 89–112, University of Esfahan, Iran.

Moritz, R., F. Ghazban, and B. S. Singer (2006), Eocene gold ore formation at Muteh, Sanandaj–Sirjan tectonic zone, Western Iran: A result of late-stage extension and exhumation of metamorphic basement rocks within the Zagros Orogen, *Econ. Geol.*, *101*, 1497–1524.

Mousivand, F., E. Rastad, S. Meffre, J. M. Peter, M. Solomon, and K. Zaw (2011), U–Pb geochronology and Pb isotope characteristics of the Chahgaz volcanogenic massive sulphide deposit, southern Iran, *Int. Geol. Rev.*, *53*, 1239–1262.

Mousivand, F., E. Rastad, S. Meffre, J. M. Peter, M. Mohajjel, K. Khin Zaw, and H. M. Emami (2012), Age and tectonic setting of the Bavanat Cu–Zn–Ag Besshi-type volcanogenic massive sulfide deposit, southern Iran, *Miner. Deposita*, *47*, 911–931.

Mouthereau, F. (2011), Timing of uplift in the Zagros belt/Iranian plateau and accommodation of late Cenozoic Arabia–Eurasia convergence, *Geol. Mag.*, *148*, 726–738.

Muttoni, G., M. Gaetani, D. V. Kent, D. Sciunnach, L. Angiolini, F. Berra, E. Garzanti, M. Mattei, and A. Zanchi (2009), Opening of the Neo-Tethys Ocean and the Pangea B to Pangea A transformation during the Permian, *GeoArabia*, *14*, 17–48.

Navabpour, P., J. Angelier, and E. Barrier (2010), Mesozoic extensional brittle tectonics of the Arabian passive margin, inverted in the Zagros collision (Iran, interior Fars), *Geol. Soc. Lond. Spec. Publ.*, *330*, 65–96, doi:10.1144/SP330.5.

Nazemzadeh, M., and A. Rashidi (2007), Geological map of Iran sheet 4347-Dehsard (Bazar), scale 1:100,000, Geological Survey of Iran, Tehran.

Nazemzadeh, M., J. Roshan Ravan, and H. Azizan (1996), Geological map of Iran sheet 7147-Baghat, scale 1:100,000, Geological Survey of Iran, Tehran.

Nazemzadeh, M., J. Roshan Ravan, and H. Azizan (1997), Geological map of Iran sheet 7247-Khabr, scale 1:100,000, Geological Survey of Iran, Tehran.

Nutman, A. P., M. Mohajjel, V. C. Bennett, and C. L. Fergusson (2014), Gondwanan Eoarchean–Neoproterozoic ancient crustal material in Iran and Turkey: Zircon U–Pb–Hf isotopic evidence, *Can. J. Earth Sci.*, *51*, 272–285, doi:10.1139/cjes-2013-0138.

Omrani, J., and A. R. Khabbaznia (2003), Geological map of Alut (scale 1:100,000), Geological Survey of Iran, Tehran, Iran.

Pamic, J., G. Sestini, and D. Adib (1979), Alpine magmatic and metamorphic processes and plate tectonics in the Zagros range, Iran, *Geol. Soc. Am. Bull.*, *90*, 569–576.

Paul, A., D. Hatzfeld, A. Kaviani, M. Tatar, and C. Péquegnat (2010), Seismic imaging of the lithospheric structure of the Zagros mountain belt (Iran), in *Tectonic and Stratigraphic Evolution of Zagros and Makran During the Mesozoic-Cenozoic*, edited by P. Leturmy, and C. Robin, *Geol. Soc. London, Spec. Publ.*, *330*, pp. 5–18.

Pessagno, E. A., A. M. Ghazi, M. Kariminia, R. A. Duncan, and A. A. Hassanipak (2005), Tectonostratigraphy of the Khoy Complex, northwestern Iran, *Stratigraphy*, *2*, 49–63.

Rachidnejad-Omran, N., M. H. Emami, M. Sabzehei, E. Rastad, H. Bellon, and A. Piqué (2002), Lithostratigraphie et histoire paléozoïque à paléocène des complexes métamorphiques de la région de Muteh, zone de Sanandaj-Sirjan (Iran méridional), *C. R. Geosci.*, *334*, 1185–1191.

Reilinger, R., and S. McClusky (2011), Nubia–Arabia–Eurasia plate motions and the dynamics of Mediterranean and Middle East tectonics, *Geophys. J. Int.*, *186*, 971–979, doi:10.1111/j.1365-246X.2011.05133.x.

Reuter, M., W. E. Piller, M. Harzhauser, O. Mandic, B. Berning, F. Rögl, A. Kroh, M. P. Aubry, U. Wielandt-Schuster, and A. Hamedani (2007), The Oligo-/Miocene Qom Formation (Iran): Evidence for an early Burdigalian restriction of the Tethyan Seaway and closure of its Iranian gateways, *Int. J. Earth Sci.*, doi:10.1007/s00531-007-0269-9.

Richards, J. P., D. Wilkinson, and T. Ullrich (2006), Geology of the Sari Gunay epithermal gold deposit, northwest Iran, *Econ. Geol.*, *101*, 1455–1496.

Ricou, E. (1970), Comments on radiolarite and ophiolite nappes in the Iranian, *Geol. Mag.*, 479–480.

Robertson, A. H. F. (2002), Overview of the genesis and emplacement of Mesozoic ophiolites in the Eastern Mediterranean Tethyan region, *Lithos*, *65*, 1–67.

Robin, C., S. Gorican, F. Guillocheau, P. Razin, G. Dromart, and H. Mosaffa, (2010), Mesozoic deep-water carbonate deposits from the southern Tethyan passive margin in Iran (Pichakun nappes, Neyriz area): Biostratigraphy, facies sedimentology and sequence stratigraphy, in *Tectonic and Stratigraphic Evolution of Zagros and Makran During the Mesozoic–Cenozoic*, edited by P. Leturmy and C. Robin, *Geol. Soc. Spec. Publ.*, *330*, pp. 179–210.

Roshan Ravan, J., S. A. Eshraghi, and M. Sabzehei (1997), Geological map of Iran sheet 7148-Sirjan, scale 1:100,000, Geological Survey of Iran, Tehran.

Sabzehei, M. (1974), Les melange ophiolitiques de la region de'Esfandagheh, These d'etate, Universite Scientifique et Medicale de Grenoble, France, 306 pp.

Sabzehei, M., J. Roshan Ravan, B. Amini, S. A. Eshraghi, S. Alai Mahabadi, and M. Seraj (1993), Geological map of the Neyriz quadrangle H-11, scale 1: 250,000 Geological Survey of Iran.

Sabzehei, M., M. Berberian, A. Houshmandzadeh, M. A. A. Nowgole-Sadat, B. Majidi, N. Alavi-Tehrani, J. Roshan Ravan, H. Azizan, and M. Nazemzadeh (1994), Hajiabad quadrangle map, 1:250,000, Geological Survey of Iran, I12.

Sahandi, M. R., J. Radfar, J. Hoseinidoust, and M. Mohajjel (2006), Geological map of Iran sheet 5857-Shazand, scale 1:100,000, Geological Survey of Iran, Tehran.

Saidi, A., M. F. Brunet, and L. E. Ricou (1997), Continental accretion of the Iran Block to Eurasia as seen from Late Paleozoic to Early Cretaceous subsidence curves, *Geodyn. Acta*, *10*, 189–208.

Sarjoughian, F., A. Kananian, M. Haschke, and A. J. Ahmadian (2015), Transition from I-type to A-type magmatism in the Sanandaj–Sirjan Zone, NW Iran: An extensional intra-continental arc, *Geol. J.*, doi:10.1002/gj.2637.

Saura, E., et al. (2011), Basin architecture and growth folding of the NW Zagros early foreland basin during the Late Cretaceous and early Tertiary, *J. Geol. Soc.*, *168*, 235–250, doi:10.1144/001676492010-092.

Sengör, A. M. C. (1979), Mid-Mesozoic closure of Permo-Triassic Tethys and its implications, *Nature*, *279*, 590–593.

Sengör, A. M. C. (1990), A new model for the late Paleozoic-Mesozoic tectonic evolution of Iran and implications for Oman, in *The Geology and Tectonics of the Oman Region*, edited by A. H. F. Robertson, M. P. Searle, and A. C. Reis, *Geol. Soc. London, Spec. Publ.*, *49*, pp. 797–831.

Sengör, A. M. C., A. Cin, D. B. Rowley, and S. Y. Nie (1993), Space-time patterns of magmatism along the Tethysides: A preliminary study, *J. Geol.*, *101*, 51–84.

Sepahi, A. A., D. L. Whitey, and A. A. Baharifar (2004), Petrogenesis of Andalusite-Kyanite-Sillimanite veins and host rocks, Sanandaj-Sirjan metamorphic belt, Hamedan, Iran, *J. Metamorph. Geol.*, *22*, 119–134.

Sepahi, A. A., S. R. Jafari, and S. Mani-Kashani (2009), Low pressure migmatites from the Sanandaj-Sirjan metamorphic belt in the Hamedan region (Iran), *Geol. Carpath.*, *60*, 107–119, doi:10.2478/v10096-009-0007-2.

Sepahi, A., H. Shahbazi, W. Siebel, and A. Ranin (2014), Geochronology of plutonic rocks from the Sanandaj-Sirjan zone, Iran and new zircon and titanite U-Th-Pb ages for granitoids from the Marivan pluton, *Geochronometria*, *41*, 207–215.

Shafaii Moghadam, H., and R. J. Stern (2011), Geodynamic evolution of upper Cretaceous Zagros ophiolites: Formation of oceanic lithosphere above a nascent subduction zone, *Geol. Mag.*, *148*, 762–801.

Shafaii Moghadam, H., X.-H. Li, X.-X. Ling, R. J. Stern, J. F. Santos, G. Meinhold, G. Ghorbani, and S. Shahabi (2015), Petrogenesis and tectonic implications of Late Carboniferous A-type granites and gabbronorites in NW Iran: Geochronological and geochemical constraints, *Lithos*, *212–215*, 266–279, doi:10.1016/j.lithos.2014.11.009.

Shahbazi, H., W. Siebel, M. Pourmoafee, M. Ghorbani, A. A. Sepahi, C. K. Shang, and M. Vousoughi Abedini (2010), Geochemistry and U–Pb zircon geochronology of the Alvand plutonic complex in Sanandaj–Sirjan Zone (Iran): New evidence for Jurassic magmatism, *J. Asian Earth Sci.*, *39*, 668–683.

Shahidi, A. (2000), Geological map of Iran sheet 7651-Jian, scale 1:100,000, Geological Survey of Iran, Tehran.

Shakerardakani, F., F. Neubauer, F. Masoudi, B. Mehrabi, X. Liu, Y. Dong, M. Mohajjel, B. Monfaredi, and G. Friedl (2015), Pan-African basement and Mesozoic gabbro in the Zagros orogenic belt in the Dorud–Azna region (NW Iran): Laser-ablation ICP–MS zircon ages and geochemistry, *Tectonophysics, 647–648*, 146–171.

Sheikholeslami, M. R., and M. Zamani Pedram (2005), Geological map of Iran sheet 6057-Mahallat, scale 1:100,000, Geological Survey of Iran, Tehran.

Sheikholeslami, M. R., A. Pique, P. Mobayen, M. Sabzehei, H. Bellon, and M. H. Emami (2008), Tectonometamorphic evolution of the Neyriz metamorphic complex, Quri-Kor-e-Sefid area (Sanandaj-Sirjan Zone, SW Iran), *J. Asian Earth Sci.*, *31*, 504–521.

Shirdashtzadeh, N., S. Kachovich, J. C. Aitchison, and R. Samadi (2015), Mid-Cretaceous radiolarian faunas from the Ashin Ophiolite (western Central-East Iranian Microplate), *Cretaceous Res.*, *56*, 110–118.

Soffel, H. C., M. Davoudzadeh, C. Rolf, and S. Schmidt (1996), New palaeomagnetic data from Central Iran and a Triassic palaeoreconstruction, *Geol. Rundsch.*, *85*, 293–302.

Soheili, M., M. B. Jafarian, and M. R. Abdolahi (1992), Geological map of Iran sheet 5956-Aligoodarz, scale 1:100,000, Geological Survey of Iran, Tehran.

Stampfli, G. M., and G. D. Borel (2002), A plate tectonic model for the Paleozoic and Mesozoic constrained by dynamic plate boundaries and restored synthetic oceanic isochrones, *Earth Planet. Sci. Lett.*, *196*, 17–33.

Stockli, D. F., J. Hassanzadeh, L. D. Stockli, G. Axen, J. D. Walker, and T. J. Dewane (2004), Structural and geochronological evidence for Oligo-Miocene intra-arc low-angle detachment faulting in the Takab-Zanjan area, NW Iran, *Abstr. Programs Geol. Soc. Am.*, *36*(5), 319.

Stöcklin, J. (1968), Structural history and tectonics of Iran: A review, *Am. Assoc. Pet. Geol. Bull.*, *52*, 1229–1258.

Stöcklin, J. (1972), *Iran Central, septentrional et oriental, Lexique Stratigraphique International, III, Fascicule 9b, Iran, 1-283*, Centre National de la Recherche Scientifique, Paris.

Stöcklin, J. (1974), Possible ancient continental margins in Iran, in *The Geology of Continental Margins*, edited by C. A. Burk and C. L. Drake, pp. 873–887, Springer, New York.

Stöcklin, J. (1981), A brief report on geodynamics in Iran, in *Zagros, Hindukush, Himalaya Geodynamic Evolution*, edited by H. K. Gupta and F. M. Delany, pp. 70–74, AGU, Washington, D. C.

Stöcklin, J., and M. H. Nabavi (1973), Tectonic map of Iran, scale 1:2500000, Geological Survey of Iran, Tehran.

Szabo, F., and A. Kheradpir (1978), Permian and Triassic stratigraphy, Zagros basin, south-west Iran, *J. Pet. Geol.*, *1*(2), 57–82.

Takin, M. (1972), Iranian geology and continental drift in the Middle East, *Nature*, *235*, 147–150.

Taraz, H. (1974), Geology of the Surmaq-Deh Bid area, Abadeh region, Central Iran, Geological Survey of Iran, 37, 148 pp.
Tatar, M., and A. Nasrabadi (2013), Crustal thickness variations in the Zagros continental collision zone (Iran) from joint inversion of receiver functions and surface wave dispersion, *J. Seismol.*, *17*, 1321–1337, doi:10.1007/s10950-013-9394-z.
Tavakoli-Shirazi, S., D. Frizon de Lamotte, J. C. Wrobel-Daveau, and J. C. Ringenbach (2013), Pre-Permian uplift and diffuse extensional deformation in the High Zagros Belt (Iran): Integration in the geodynamic evolution of the Arabian plate, *Arab. J. Geosci.*, *6*, 2329–2342, doi:10.1007/s12517-012-0542-5.
Thiele, O., M. Alavi, R. Assefi, A. Hushmandzadeh, K. Seyed-Emami, and M. Zahedi (1968), Explanatory text of the Golpaygan quadrangle map, 1:250,000, Geological Survey of Iran, E7, 24 p.
Tillman, J. E., A. Poosti, S. Rossello, and A. Eckert (1981), Structural evolution of Sanandaj-Sirjan Ranges near Esfahan, Iran, *Am. Assoc. Pet. Geol. Bull.*, *65*, 674–687.
Timotijevic, S., S. Cvetic, M. N. Dimitrijevic, and M. D. Dimitrijevic (1972), Geological map of Iran sheet 7447-Esfandaqeh, scale 1:100,000, Geological Survey of Iran, Tehran.
Valizadeh, M. V., and J. M. Cantagrel (1975), Premieres donnees radiometriques (K-Ar et Rb-Sr) sur les micas du complexe magmatique du Mont Alvand, Hamadan (Iran occidental), *C.R. Acad. Sci. Paris*, *281*, 1083–1086.
Valizadeh, M. V., and S. Zarian (1976), A study of petrology of the Almogholagh pluton, Asadabad, Hamadan, *Univ. Tehran J. Sci.*, *8*, 49–59 (in Farsi).
Verdel, C., B. P. Wernicke, J. Ramezani, J. Hassanzadeh, P. R. Renne, and T. L. Spell (2007), Geology and thermochronology of Tertiary Cordilleran-stylemetamorphic core complexes in the Saghand region of central Iran, *Geol. Soc. Am. Bull.*, *119*, 961–977.
Verdel, C., B. P. Wernicke, J. Hassanzadeh, and B. Guest (2011), A Paleogene extensional arc flare-up in Iran, *Tectonics*, *30*, TC3008, doi:10.1029/2010TC002809.
Verdel, C., J. Hassanzadeh, B. Wernicke, and A. D. Stockli (2013), The Eocene Golpaygan metamorphic core complex, Central Iran: A case history of orogen-parallel forearc rifting along an Andean-type continental margin, *Geol. Soc. Am. Abstr. Progr.*, *45*(7), 516.
Vernant, P., et al. (2004), Present-day crustal deformation and plate kinematics in the Middle East constrained by GPS measurements in Iran and northern Oman, *Geophys. J. Int.*, *157*, 381–398, doi:10.1111/j.1365-246X.2004.02222.x.
Watters, W. A., M. Sabzehei, M. Alavi Tehrani, H. Etminan, and B. Majidi (1970), Preliminary report on the geology and petrography of the metamorphic and igneous rocks of central part of Neyriz Quadrangle, *Geological Survey of Iran*, Internal report, 113 pp.
Whitechurch, H., J. Omrani, P. Agard, F. Humbert, R. Montigny, and L. Jolivet (2013), Evidence for Paleocene–Eocene evolution of the foot of the Eurasian margin (Kermanshah ophiolite, SW Iran) from back-arc to arc: Implications for regional geodynamics and obduction, *Lithos*, *182–183*, 11–32.
Yin, A. (2010), Cenozoic tectonic evolution of Asia: A preliminary synthesis, *Tectonophysics*, *488*, 293–325, doi:10.1016/j.tecto.2009.06.002.
Zahedi, M. (1976), Explanatory text of the Esfahan quadrangle map, 1:250,000, Geological Survey of Iran, F8, 49 pp.
Zahedi, M. (1991), Explanatory text of the Kashan quadrangle map, 1:250,000, Geological Survey of Iran, F7, 98 pp.
Zahedi, M. (1993), Shahrekord quadrangle map, 1:250,000, Geological Survey of Iran, E8.